Geochemical and Hf-Nd isotope data of Nanhua rift sedimentary and volcaniclastic rocks indicate a Neoproterozoic continental flood basalt provenance

Xuan-Ce Wang[1, 2]* Zheng-Xiang Li[1] Xian-Hua Li[2] Qiu-Li Li[2] Qi-Rui Zhang[2]

1. The Institute for Geoscience Research, Department of Applied Geology, Curtin University, GPO Box U1987, Perth, WA 6845, Australia

2. State Key Laboratory of Lithospheric Evolution, Institute of Geology and Geophysics, Chinese Academy of Sciences, P.O. Box 9825, Beijing 100029, China

* Corresponding author. Present address: Department of Applied Geology, Curtin University, GPO Box U1987, Perth, WA 6845, Australia.

Phone: +61 8 9266 2453

Fax: +61 8 9266 3153

E-mail: X.Wang3@curtin.edu.au (X.C.Wang)

Abstract

Geochemical and Hf-Nd isotope studies of Neoproterozoic sedimentary and volcaniclastic rocks in the Nanhua Rift Basin, South China, demonstrate that their source provenances contained large proportions of mafic rocks and various amounts of granites. A significant proportion of the studied Neoproterozoic rift sedimentary and volcaniclastic rocks have initial εNd(t) values higher than those of Neoproterozoic granites, but fall within the range of ca. 825–750 Ma basaltic rocks. Their initial εNd(t) values correlate with ratios of La/Sc, La/Cr, La/V, La/Co and La/Ni. The Nd isotope and trace element data, in combination with existing in-situ U-Pb and hafnium-oxygen isotope analyse of the detrital zircon grains indicate a dominant ca. 825–800 Ma mafic provenance. Furthermore the Hf-Nd isotopic compositions of the studied samples plot within the field of the remanent of ca. 825–810 Ma continental flood basalts and form a linear array that passes through the average value of the remnant ca. 825–810 Ma continental flood basalts. Thus, the inferred large proportions of mafic rocks in the source provenance of the Neoproterozoic rift sedimentary and volcaniclastic rocks likely signify an eroded continental flood basalt province, similar to that reported for the Neoproterozoic sedimentary rocks in Australia. This work thus provides further evidence for the possible once existence of a common large igneous province between South China and eastern Australia as adjacent parts of the supercontinent Rodinia.

Keywords: Nanhua Rift Basin; Neoproterozoic; provenance; Hf-Nd isotopes; continental flood basalts; Rodinia

1. Introduction

Continental flood basalt (CFB) provinces, an on-land member of large igneous provinces (LIPs), have significant implications for continental growth, rifting and breakup (e.g., Hill et al., 1992; Saunders et al., 1996). Neoproterozoic LIPs and associated CFBs are a key source of information for Rodinia reconstructions (e.g., Ernst et al., 2008; Li et al., 2008b; Wang et al., 2010b). However, studies of ancient CFBs are often hindered by their sporadic preservation due to continental erosion. This is especially true because the positive relief formed above an ascending plume head is normally where the CFB is located (e.g., Hill et al., 1992). Volcanic rocks formed during the later stages of an eruption cycle are even more susceptible to erosion as these upper units would be the first to be stripped away when the volcanic systems became dormant.

Continental doming is demonstrated to have occurred during the Neoproterozoic plume events in South China (Li et al., 1999). Rapid continental doming and unroofing are the controlling factor in eroding away most of the Neoproterozoic CFB provinces in South China and Australia (Li at al., 1999, 2008b; Barovich and Foden, 2000; Wang et al., 2008, 2010b). Although eroded CFBs may be lost from the volcanic record, their chemical signatures can be preserved in adjacent sedimentary basins (e.g., Barovich and Foden, 2000). Thus, geochemical and isotopic parameters that are sensitive to source provenance but insensitive to chemical weathering, hydraulic fractionation and sorting processes can be used to reveal the eroded CFB provinces (e.g., Barovich and Foden, 2000). Particularly, immobile elements such as

Al, Fe, Ti, Th, Sc, Co, Zr, rare earth elements (REEs) and Nd isotopes have been found to be useful indicators of the source provenance (e.g., Taylor and McLennan, 1985; Barovich and Foden, 2000; Singh, 2009 and references therein).

The configuration and breakup history of the Neoproterozoic supercontinent Rodinia are still debated partly because the related magmatic records are highly fragmentary and incomplete (Li et al., 2008b and references therein). South China and southern-central Australia have some of the best-preserved Neoproterozoic sedimentary records related to the breakup of Rodinia (e.g., Li et al., 2008b and references therein; Fig. 1A). Geochemical and Nd isotope studies of Neoproterozoic sedimentary successions in southern-central Australia provided important constraints on the once existence of a widespread Neoproterozoic CFB province related to the breakup of Rodinia (e.g., Barovich and Foden, 2000). If the two continents were indeed adjacent to each other in Rodinia as proposed by Li et al. (1995, 1999, 2003b, 2008b), the plume-induced CFB province (e.g., Ernst et al., 2008; Li et al., 2008b; Wang et al., 2007a, 2008, 2009, 2010b) could have served as the source provenance not only for Neoproterozoic sediments in Australian rift basins, but also for their counterparts in South China. Therefore, similar geochemical and isotope records are expected from the Neoproterozoic sedimentary rocks in South China.

We present here a comprehensive geochemical and Hf-Nd isotopic study of Neoproterozoic rift sediments in the Nanhua Rift of the South China Block, a major Neoproterozoic continental rift system in the world. The goal of this study is to use the geochemical and Hf-Nd isotopic compositions of the sediments to understand the sedimentation history of the basin in light of their source rock characteristics. Such information will provide a further test on the hypothesized existence of widespread CFBs in the South China Block during the breakup of Rodinia, and the possible relationship between South China and Australia in Rodinia.

2. Geological settings

Two major Neoproterozoic clastic sedimentary sequences were deposited in South China after the ca. 1.1–0.9 Ga Sibao orogeny (Fig. 1B) (e.g, Li et al., 2002b, 2007c, 2008b, 2009a; Ye et al., 2007) but prior to the first glacial interval (the Chang'an Formation): the Sibao/Lengjiaxi Group (sequence-set I in Fig. 2) and the overlying Xiajiang/Danzhou/Banxi Group (sequence-set II in Fig. 2). The two sequences are commonly in unconformable contact (Fig. 2; Wang and Li, 2003). Whereas the lower sequence is still poorly studied and its tectonic significance yet unclear, the younger sequence is well preserved as wedge-shaped continental rift successions that consist of continental and marine siliciclastic and volcaniclastic rocks interbedded with bimodal volcanic rocks and tuff (e.g., Li et al., 2002a; Wang and Li, 2003). These strata are distributed in three major Neoproterozoic continental rift systems in South China: the roughly E-W trending Bikou-Hannan Rift along the northwestern margin of the Yangtze Block, the N-S trending Kangdian Rift near the present western margin of the Yangtze Block, and the major NE-SW trending Nanhua Rift to the southeast (Fig. 1B). The onset of this rift sequence has been dated at ca. 820 Ma (Wang et al., 2003; Li et al., 2008b and references therein) (Fig. 2). This event was accompanied by widespread anorogenic magmatism including the 823 ± 12 Ma

Yiyang anhydrous high-Mg basalts (Wang et al., 2007a), the Bikou-Tiechuanshan CFBs (Ling et al., 2003; Wang et al., 2008), sporadic basalt outcrops (e.g., Li et al, 2002a, 2005, 2008a; Zhou et al., 2002a, 2009; Wang et al., 2009), mafic dyke swarms (e.g., Li et al.,1999), mafic-ultramafic complexes (Zhou et al., 2002b, 2006; Zhu et al., 2007), and numerous synchronous granitic intrusions in both the interior and along the margins of the Yangtze Block (Li et al., 2003a; Wang et al., 2010b) and adjacent regions. These ca. 825–800 Ma basaltic magmatism and synchronous felsic igneous rocks are collectively called the Guibei LIP (e.g., Li et al., 1999, 2008b; Ernst et al., 2008; Wang et al., 2010b; see recent update at http://www.largeigneousprovinces.org/09may.html). The initiation of this rift sequence was associated with a large-scale syn-magmatic doming (Li et al., 1999).

The Nanhua Rift Basin is the largest failed continental rift basin in the South China Block (e.g., Wang and Li, 2003) (Fig. 1B). The rift successions near the northwestern margin of the rift basin (Figs. 1B, 1C and 2) are well exposed and well studied. The laterally correlatable rift successions there are called the Banxi Group in Hunan Province, the Xiajiang Group in eastern Guizhou Province, and the Danzhou Group in northern Guangxi Province (e.g., Wang and Li, 2003) (Figs. 1 and 2). Wang and Li (2003) divided the pre-725 Ma Neoproterozoic rift successions into two sequence-sets (II-1 and II-2 in Fig. 2). The deposition age for the first sequence-set (II-1 in Fig. 2) was estimated at ca. 820–800 Ma (Wang and Li, 2003) although more recent age data put the younger age limit to ca. 790 Ma (Wang et al., 2011a). The thickness of the rift successions in eastern Guizhou Province is up to 10,000 m, although some of the thickness estimations may have neglected structural duplications. The Neoproterozoic rift sequences in this area are therefore the best candidate for investigating the characteristics of the source provenance for the Nanhua Rift Basin sedimentary rocks.

Thirty-five of the 51 samples analysed during this study were from the Xiajiang Group in southeastern Guizhou Province (Figs. 1C and 2). The Xiajiang Group is largely composed of thick siliciclastic rocks, tuff and carbargilite (Fig. 2). It was subdivided into six formations in southeastern Guizhou: the Jialu, Wuye, Fanzhao, Qingshuijiang, Pinglue and Longli formations (Fig. 2). The Jialu and Wuye formations, the lower part of the Xiajiang Group (Fig. 2), were formed during the early stage of the rifting with a low depositional rate (e.g., Wang and Li, 2003; Wang et al., 2006; Zhang et al., 2009). The Jialu Formation consists of fluvial/alluvial clastic rocks interbedded with volcaniclastic rocks, with a basal conglomerate unit overlying either unconformably over the Sibao Group clastic rocks or over granitic intrusions. The upper Jialu Formation consists of calcareous rocks, overlain by shales in the Wuye Formation. The upper part of the Xiajiang Group consists of the remaining four formations (II-2 in Fig. 2) and represents the rapid basin-filling stage (Wang and Li, 2003). This sequence-set is characterized by high depositional rate and multiple intervals of volcanic rocks. Its age spread is estimated at ca. 800 to 750–725 Ma (e.g., Wang and Li, 2003; Yin et al., 2007; Zhang et al., 2008a, b).

In addition, four samples (08SC53–08SC56) are from the Jiangkou Group (the Sturtian glacial deposit equivalent) in eastern Guangxi Province, near Liping (Figs.

1C, 2).

Four out of the 51 samples (08SC70, 08SC71-1, 08SC74 and 08SC75) were from the Danzhou Group in northern Guangxi Province (Figs. 1C, 2). The Group consists of four formations (Fig. 2) with a total stratigraphic thickness varying between ~1,000 m and ~3,400 m. The Baizhu Formation at the bottom of the succession is characterized by fluvial/alluvial clastic rocks, volcaniclastic rocks and carbonates, whereas the Hetong Formation is dominated by shale (Wang and Li, 2003). The upper part of the Danzhou Group consists of the Sanmenjie and Gongdong formations. The Sanmenjie Formation mainly consists of marine volcanic and clastic rocks, whereas the Gongdong Formation is dominated by littoral to shallow-marine siliciclastic rocks (e.g., Wang and Li, 2003). One sample (08SC68-1) was collected from the Sibao Group in this region (Figs. 1C, 2).

Four samples (08SC08–08SC11) were collected from the Yanmenzhai Formation at the top of the Banxi Group in southwestern Hunan Province (Figs. 1C, 2). The Banxi Group has a maximum thickness of >3,500 m which thins rapidly toward the rift shoulder (Zhang et al., 2008b). The age span of the Banxi Group has been defined to be between 814 ± 12 Ma (Wang et al., 2003) and 725 ± 10 Ma (Zhang et al., 2008a) (Fig. 2). In addition, three glacial deposit samples (08SC14–08SC16) were from the lower part of Chang’an Formation (the lower part of Jiangkou Group) in Hunan Province (Figs. 1C and 2).

3. Analytical techniques

Samples collected for this study are dominantly pelites, siltstone, and some volcaniclastic rocks and sandstone (Fig. 2 and Appendix A). Care was taken in sampling fresh outcrops only so to avoid the effects of weathering and hydrothermal alteration.

Samples were sawn into slabs and the central parts (>200 g) were used for bulk-rock analyses. The rocks were crushed into small fragments (<0.5 cm in diameter) before being further cleaned and powdered in a corundum mill. Bulk rock major and trace elemental analyses were conducted at the Guangzhou Institute of Geochemistry, Chinese Academy of Sciences.

Bulk-rock major element oxides were analyzed by X-ray fluorescence (XRF), following the analytical procedures described in Goto and Tatsumi (1996). A pre-ignition method was used to determine the loss on ignition (LOI) prior to major element analyses. Calibration lines used in quantification were produced by bi-variant regression of data from 36 reference materials encompassing a wide range of silicate compositions. Analyses of USGS standard reference materials (GSR-1, GSR-2, GSR-3, and GSR-5) indicate that analytical uncertainties are better than 3% for SiO_2, Al_2O_3, Fe_2O_3, MgO, Na_2O and K_2O and better than 5% for TiO_2, CaO, MnO and P_2O_5 (Appendix B Table R1).

Trace elements were analyzed using inductively coupled plasma-mass spectrometry (ICP-MS, Perkin-Elmer Sciex ELAN 6000 ICP-MS), following analytical procedures described in Li (1997) and Liu et al. (1996). About 40 mg sample powders were dissolved in high-pressure Teflon bombs using a $HF+HNO_3$ mixture. An internal standard solution containing the single element Rh was used to monitor signal drift during analysis. A set of USGS standard rocks including BHVO-2, AGV-1, GSR-1, GSR-2, GSR-3, W-2, SY4, and SARM-4 was chosen as external calibration standards for calibrating element concentrations in the measured samples. The uncertainty for most trace elements analysed is < 2%. Reproducibility, based on replicate digestion of samples, is better than 10 % for most analyses. The results of trace elemental analyses of China nature river sediment standards (GSD-9, GSD-10 and GSD-10) and two USGS standard rocks (BHVO-2 and GSR-1) (Appendix B Table R2) show that the obtained results are in good agreement with the recommended values.

Nd isotopic compositions were determined using a Micromass Isoprobe multi-collector ICP-MS (MC-ICP-MS) at the Guangzhou Institute of Geochemistry, following analytical procedures described in Li et al. (2004). Nd fractions were separated by passing through cation columns followed by HDEHP columns, and the aqueous sample solution was taken up in 2% HNO_3 and introduced into the MC-ICP-MS using a Meinhard glass nebuliser with an uptake rate of 0.1 ml/min. The inlet system was cleaned for 5 min between analyses using high purity 5% HNO_3 followed by a blank solution of 2% HNO_3. Measured $^{143}Nd/^{144}Nd$ ratios were normalized to $^{146}Nd/^{144}Nd = 0.7219$, and the reported $^{143}Nd/^{144}Nd$ ratios were further adjusted relative to the Shin Etsu JNdi-1 standard of 0.512115, corresponding to the La Jolla standard of 0.511860 (Tanaka et al., 2000).

For Hf isotopic analyses, ca. 100 mg rock powders were homogeneously mixed with 200 mg $Li_2B_4O_7$. The mixtures were digested for 15 minutes at 1200 °C in Pt–Au crucibles, then dissolved in 2M HCl. Hf fractions were separated following a modified single-column separation procedure through ion exchanges using an Eichrom® Ln-Specresin following the procedure of Li et al. (2007a). Hf isotopic ratios were analysed on a Finnigan Neptune MC-ICP-MS at the State Key Laboratory of Lithospheric Evolution, Institute of Geology and Geophysics, Chinese Academy of Sciences. Measured $^{176}Hf/^{177}Hf$ ratios were normalized to $^{179}Hf/^{177}Hf = 0.7325$, and the reported $^{176}Hf/^{177}Hf$ ratios were further adjusted relative to the JMC-475 standard ($^{176}Hf/^{177}Hf = 0.282160$).

During the course of this study, international standard rocks BHVO-2, JB-1 and JB-3 yielded (1) $^{176}Hf/^{177}Hf = 0.283097 \pm 11$ (2σ, n = 4), 0.282974 ± 7 (2σ, n = 4), 0.282974 ± 7 (2σ, n = 2), respectively; and (2) $^{143}Nd/^{144}Nd = 0.512973 \pm 10$ (2σ, n = 4), 0.512779 ± 5 (2σ, n = 4), 0.513062 ± 13 (2σ, n = 2), respectively. These measured values are in good agreement within reported errors with the recommended values (Appendix B Table R3).

4 Results

4.1 Major elements

Major element data are shown in Appendix A and Figures 3–5. In terms of major element compositions, the Neoproterozoic sedimentary rocks on the whole are characterized by intermediate SiO_2 contents (SiO_2 = 57–80 wt.%, mostly 60–70 wt.%), variable K_2O/Na_2O ratios (0.01–44, typically 0.1–3), and relatively high Fe_2O_3* + MgO contents (usually 4–10 wt %, average 8 wt %; Fe_2O_3* represents total iron as

Fe_2O_3). Most samples have low CaO contents (typically <1 wt %) and high $Al_2O_3/(Na_2O + CaO)$ ratios (typically >3), indicating either a dearth of original carbonate minerals or depletion of CaO and Na_2O during diagenetic/metamorphic processes. K_2O/Al_2O_3 ratios in all samples are below 0.3, with an average of 0.16 ± 0.08, similar to the range of clay mineral values (0 to 0.3; Cox et al., 1995). Moreover, the samples are characterized by good to moderate correlations of (1) SiO_2 with Al_2O_3 (correlation coefficient r = 0.90), Fe_2O_3* (r = 0.59), K_2O (r = 0.68) and MgO (r = 0.50); and (2) Al_2O_3 with TiO_2 (r = 0.57) and K_2O (r = 0.81) (Fig. 3 and Appendix C).

The studied samples are characterized by relatively low SiO_2/Al_2O_3 (mostly < 7) and $Fe_2O_3^*/K_2O$ (mostly < 3.0) ratios. Using the geochemical classification diagram of Herron (1988), the sedimentary rocks are classified as shale and wacke, except for four samples that fall within the Fe-sand field (Fig. 5).

4.2. Large ion lithophile elements (LILEs)

The ranges for median concentrations of Rb and Sr are 1–190 and 10–388 ppm, respectively (Appendix A). The samples display highly variable Ba contents, from 10 to 1579 ppm (mostly >400 ppm and with the average of 748 ppm) (Appendix A). Like K_2O, Rb and Ba also correlate with Al_2O_3 (r = 0.76 and 0.75, respectively), indicating that these elements were incorporated into clays during chemical weathering. In contrast, CaO, Na_2O, and Sr display highly negative correlations with the chemical index of alteration (CIA= $[Al_2O_3/(Al_2O_3 + CaO^* + Na_2O + K_2O)]*100$, mole fraction; Nesbitt and Young, 1984), suggesting that these elements were leached during chemical weathering. Rb and Ba in the studied samples correlated with SiO_2 (r = -0.71 and -0.62, respectively; Appendix C).

4.3 High field strength elements (HFSEs)

Average contents of Zr, Hf, Nb, Ta, Y, Th and U for the studied samples are 248, 7, 12, 0.93, 35, 10, and 2 ppm, respectively. HFSEs show good correlations with Al_2O_3 and SiO_2 and consistent inter-relationships (see Appendix C). Zr/Hf ratios range from 29 to 39. Nb/Ta ratios vary from 11 to 16, with an average of 13.5. Nb/Ta ratios for the studied samples are slightly higher than that of the bulk continental crust (~12–13; Barth et al., 2000) and PAAS (~12; Barth et al., 2000).

4.4 Transition trace elements (TTE)

The abundances of transition trace elements, Co (0.7–48 ppm), Cr (28–118 ppm), Ni (10–129 ppm), Sc (8–29 ppm), and V (31–169 ppm) and the ratios of Cr/Ni (0.70–7.5), Ni/Co (typically 1–5), Sc/Ni (0.28–1.40), and Sc/Cr (0.10–0.93) are variable. Transition trace elements display moderate to weak correlations with SiO_2, TiO_2, Al_2O_3 and MgO (Figs. 3-4; Appendix C).

4.5 Rare earth elements (REE)

The REEs are considered to be essentially uniform in abundances in fine-grained clastic sedimentary rocks and are not easily affected by weathering, diagenesis, or most forms of metamorphism (e.g., Taylor and McLennan 1985). The Nanhua Rift sediments, when plotted on chondrite-normalised diagrams (Fig. 6), show LREE (light REE) enriched and HREE (heavy REE) depleted patterns (La_N/Yb_N = 4 to 16, typically 6–10, where subscript N denotes chondrite normalization). The total REE abundances of the studied samples range from 68 to 496 ppm, with an average of 204 ppm, comparable to those of cratonic shales (total REE = 133 to 175 ppm; Condie, 1993). All the samples show intermediate to negligible negative Eu-anomalies, with Eu-anomalies ($Eu/Eu^* = Eu_N/(Sm^*Gd)_N^{0.5}$) ranging from 0.44 to 0.88 and with an average of 0.72 ± 0.08 (2σ) (Appendix A), which are significantly higher than the average value of typical granitic rocks (<0.5; Condie, 1993) and those of ca. 825–780 Ma granites from South China that have an average Eu*/Eu value of 0.43 ± 0.20 (n = 90; Li et al., 2003a; Wang et al., 2010a and references therein). The Eu*/Eu values of the studied samples are slightly lower than those of 825–800 Ma basalts from South China that have an average of 0.93 ± 0.13 (2σ, n = 86; Wang et al., 2009 and references therein). Both LREEs (La-Eu) and HREEs (Gd-Lu) show variable fractionation with $(La/Sm)_N$ values ranging between 1.1 and 6.1 (typically 3–5, averages 3.5; Appendix A). $(Gd/Yb)_N$ values range between 0.6 and 2.0 (typically 1.2–1.8, average 1.4). REEs show moderate to good correlations with SiO_2, Al_2O_3 and K_2O (Appendix C).

4.2 Nd and Hf isotopes

After petrographic examination and whole rock element analyses, thirty-six less-altered samples were selected for Nd and Hf isotopic analyses. Nd and Hf isotope results are presented in Tables 1–2 and Figures 7–10. All but four of the $^{147}Sm/^{144}Nd$ ratios fall in the range of 0.10–0.13. The ranges of εNd(0) values are from -5.0 to -15.5 with the majority falling between -10 and -15. Initial εNd(t) values range from +2.8 to -6.9, typically from 0 to -6 (Fig. 7B). Sediments from all the formations have similar initial εNd(t) values (Table1). Figure 8 shows that there is a sharp increase in initial εNd(t) values during the Neoproterozoic (ca. 825–700 Ma). The studied sediments are characterized by negative correlations of εNd(t) with La/Sc, La/V, La/Cr, La/Co, and La/Ni (r ranging from -0.52 to -0.64; Fig. 9).

All but four measured $^{176}Lu/^{177}Hf$ ratios range from 0.011 to 0.017, with the majority falling between 0.012 and 0.015. These sedimentary rocks have large range of $^{176}Hf/^{177}Hf$ = 0.282241–0.282709, corresponding to the initial εHf(t) = +6.4 to -9.2. The Hf isotopes in the studied sediments tightly correlate with their Nd isotopes. The Hf-Nd isotopic data defines a single coherent trend as defined by equation εHf(t) = 1.48εNd(t) +3.95, R^2 = 0.84 (Fig. 10).

5. Discussion

5.1. Hydraulic sorting and quartz dilution

The correlations between selected elements versus Al_2O_3 (mica and clays), P (apatite) and Zr (zircon) can be used to evaluate the control of geochemical compositions by clays or micas versus heavy mineral fractions in sediments (e.g., Taylor and McLennan, 1985; Cullers et al., 1988; McLennan et al., 1990). Such correlations (Fig. 3 and Appendix C) indicate that (1) aluminous minerals (e.g., mica and clays) played an important role in controlling the geochemical compositions of the studied samples; (2) Ti-bearing Fe phases (e.g., ilmenite) may have contributed to heavy mineral fractions; (3) phosphate phases within the studied sediments made minor, if any, contribution to the REE budget; and (4) zircon has played insignificant roles in controlling the LREEs budget and in HREEs fractionation. The "terrestrial array”-type linear trend of εHf vs εNd (Fig. 10) confirms that the studied sedimentary rocks underwent insignificant zircon fractionation (e.g., Bayon et al., 2009).

The negative correlations between SiO_2 and most major and trace elements (Appendix C) signify the effects of quartz dilution (e.g., Ugidos et al. 1997). However, important trace element ratios, as provenance indicators, were not significantly affected by hydrodynamic sorting. As shown in Figure 9, the fine-grained samples (pelites, tuffs and siltstones) and sandstones have similar trace element ratios of La/Sc, La/V, La/Cr, La/Co, and La/Ni.

5.2. Geochemical changes related to weathering

Palaeoweathering in the source area is one of the important processes affecting the geochemical compositions of fine-grained clastic sediments (e.g., Nesbitt and Young, 1984; Nesbitt et al., 1990). Plotting CIA values in A (Al_2O_3)–CN (CaO*+Na_2O)–K (K_2O; all in molecular proportions) compositional space can more effectively discriminate between chemical weathering, transportation, diagenesis, metamorphism and source composition of clastic sediments (e.g., Nesbitt and Young, 1984; Fedo et al., 1995). CaO* is defined as CaO in silicates only. However, in this study there was no objective way of distinguishing carbonate CaO from silicate CaO. Therefore, the total CaO values are plotted here. This is justified on the basis that none of the samples appeared calcareous, and most samples contained less than 0.8 wt.% CaO (Appendix A).

Figure 11 shows the A-CN-K plot of the fine-grained sedimentary rocks (pelite, tuff and siltstone). They define a distinct linear array that connects the plagioclase and illite end-members. Such a linear array departs significantly from the predicted weathering trends in the A-CN-K space (lines “A1” and “A2” in Fig. 11B), suggesting that these samples were affected by K-metasomatism (e.g., Fedo et al., 1995). Figure 11 also shows that the CIA values for the premetasomatized samples spread from 63 to 90 (zone 1 in Fig. 11A). All fine-grained samples lie above the feldspar join, reflecting the scarcity of feldspar in these rocks. The intersections of the inferred chemical weathering trends with the feldspar join (Fig. 11B) imply that the source rocks for the studied samples were likely enriched in plagioclase (e.g., Fedo et al., 1995).

5.3. A mafic rock dominated provenance

Li and McCulloch (1996) proposed that the source of the Neoproterozoic rift sediments in South China included a large proportion of juvenile materials, as indicated by a sharp decrease in Nd model ages and an increase in εNd(t) values (e.g., Li and McCulloch, 1996; Wu et al., 1998). As shown in Figure 8, the Sibao Group, with maximum stratigraphic age of about 850 Ma (Gao et al., 2010b), has initial εNd(t) values ranging from -6 to -7. In contrast, the mid-Neoproterozoic (ca. 820–730 Ma) Nanhua Rift sediments have significantly higher initial εNd(t) values of up to +3. In the younger, Sinian sediments, initial εNd(t) values decreased to below -6. Although the prominent positive “Nd isotope drift” in the mid-Neoproterozoic sedimentary rocks was previously interpreted to reflect an influx of juvenile materials in their source provenance (Li and McCulloch, 1996), the nature of the juvenile materials remained unclear.

Ca. 830–820 Ma granites, such as the Sanfang, Bendong, and Yuanbaoshan granites in Figure 1C, could have contributed to the isotopic signature of the Nanhua Rift sediments. However, a large proportion of the studied samples have initial εNd(t) values higher than that of these granites (highlighted by the grey band in Fig. 7). Their initial εNd(t) values overlap with those of the ca. 825–750 Ma basaltic rocks from the South China Block (Fig. 7). This indicates a juvenile provenance with a significant mafic component.

Transition trace elements (Sc, Cr, Ni, Co and V) and their relationships with Nd isotopes provide important constraints on the source provenance of sedimentary rocks (e.g., Taylor and McLennan, 1985; Barovich and Foden, 2000). The studied samples are characterized by correlations of Cr, Sc, V and Th/Sc versus MgO (Fig. 4), indicating an end-member enriched in Sc, Cr, V and MgO, a typical characteristic of mafic rocks. The studied samples plot mainly within the field of ca. 825–750 Ma basaltic rocks from the South China Block (Fig. 9). Furthermore, the samples form linear arrays between ratios of La/Sc, La/Cr, La/V, La/Co, and La/Ni and εNd(t) with r values ranging from -0.52 to -0.68 (Fig. 9). All the linear arrays pass through the average value of ca. 825–750 Ma basaltic rocks, similar to the average value of the remnant ca. 825–810 Ma Bikou-Tiechuanshan CFBs (Fig. 9). This suggests a mafic rock dominated provenance for the studied samples.

Apart from the mafic end-member, the linear arrays as shown in Figure 9 also imply a granitic end-member. This constraint is consistent with the bimodal nature of the ca. 825–750 Ma magmatic record in the South China Block (Li et al., 2008b and references therein). The mafic end-member is characterized by low ratios of La/Sc, La/Cr, La/V, La/Co, and La/Ni and high initial εNd(t) values. Its composition was estimated using the average of the ca. 825-750 Ma basaltic rocks in the South China Block. In contrast, the granitic end-member features high La/Sc, La/Cr, La/V, La/Co and La/Ni, and relatively low initial εNd(t) values. As shown in Figure 9, the chemical and isotopic variations of the studied samples can be attributed to a mixing of mafic and granitic rocks.

Based on these end-member compositions, mass balance calculations suggest that about 50% of the studied samples require more than 30% mafic rocks in their source provenance to achieve their chemical and Nd isotopic signatures (Fig. 9). Residual ca. 825–750 Ma basaltic rocks in South China exhibit a wide range of chemical and isotopic compositions, with εNd values ranging from about -10 to higher than +4 and La/Sc, La/Cr, La/V, and La/Ni ratios covering the whole range of the studied samples. This would thus have resulted in an underestimation of detrital contributions by such basaltic rocks. In fact, about 50% of our studied samples plot within the field defined by the ca. 825–750 Ma basaltic rocks, indicating a dominant basaltic provenance. Detrital zircon grains from the Nanhua Rift succession (samples 08SC07, 08SC11, 08SC31 and 08SC74) showed that ca. 825–800 Ma is the most dominant age group (fig. 10a of Wang et al., 2011a) and they are characterized by mantle-like $\delta^{18}O$ values (about 73% of all analyses gave values of 4.0–6.5‰; Wang et al., 2011b) and positive εHf(t) values (≥60% of all analyses; Wang et al., 2011a). All these evidence indicate a dominant ca. 825–800 Ma mafic provenance.

However, the εNd(t) values of the studied samples do not correlate with Eu/Eu* values. The following factors may have disturbed the expected correlation of εNd(t) with Eu/Eu*. First, the ca. 825–750 Ma granites from South China display a large range of Eu/Eu* values (varying between 0.02 and 0.82). Second, the ca. 825–750 Ma basaltic rocks in South China also have variable Eu/Eu* values ranging from 0.62 to 1.18 (Wang et al., 2009 and references therein). Even some less-evolved basaltic samples also display small but significant negative Eu anomalies on the REEs distribution patterns. For example, Eu/Eu* values for the ca. 825 Ma Yiyang komatiitic basalts with MgO > 10 wt.% are as low as 0.64 (calculated from data in appendix table R2 of Wang et al., 2007). Third, Eu^{2+} behaves similarly to Sr^{2+}, and is mobile during weathering and alteration. Thus, Eu/Eu* values in sedimentary rocks may reflect the integrated effect of source rocks, weathering and alteration processes. For instance, REEs data from the weathering profile of late-Cenozoic basalts in Hainan Island (South China) show that the weathering process can reduce Eu/Eu* values from ~1.0 in fresh basalts to ~0.7 in weathering products (re-calculated from table 1 of Ma et al., 2007). Thus, both the geochemical diversity of Eu/Eu* values for the two end-members, and the effects of weathering processes, could have contributed to the poor correlation between Eu/Eu* and εNd(t).

5.4. Record of eroded continental flood basalts?

The lithostratigraphic characteristics and basin geometry of the Banxi, Xiajiang, and Danzhou groups, along with widespread bimodal magmatism from ca. 830 to 745 Ma in South China, indicate that they were deposited in a rift basin (the Nanhua Rift Basin; Li et al., 1999, 2002a, 2003b; Wang and Li, 2003) that started at ca. 820 Ma between the Yangtze and Cathaysian blocks. The recently reported presence of the ca. 850–830 Ma bimodal intraplate magmatism (Li et al., 2010a and references therein) suggests that restricted rifting in South China probably started by 850 Ma (Li et al., 2010a, b). The mafic rocks have intraplate geochemical affinities (e.g., OIB-type trace element patterns) and were thought to be related to mantle plume activity in response to a circum-Rodinia mantle avalanche after the final assembly of the supercontinent (e.g., Li et al., 2008b; Li and Zhong, 2009). This plume/rifting model for the mid-Neoproterozoic magmatism and basin formation in South China contradicts the island-arc model by Li and McCulloch (1996) and Gu et al. (2002), which was mainly based on the juvenile Nd isotopic signature and geochemical tectonic discrimination diagrams. Furthermore, the island-arc model is inconsistent with a number of other geological, geochemical and petrological observations (e.g., Li et al., 1999, 2002a, 2003a, b, 2006, 2007b, 2009, 2010a, b, and c; Wang and Li, 2003; Wang et al., 2007a, 2008, 2009, 2010a, b). Petrological evidence for the ca. 825-800 Ma plume-induced Guibei LIP came from the identification of anhydrous high MgO basaltic rocks such as the 823 ± 6 Ma Yiyang lavas with primary MgO content of about 20 wt.% (#16 in Fig. 1B; Wang et al., 2007a), the ca. 800 Tongde high-Mg picrite dike with primary MgO > 21 wt.% (#10 in Fig. 1B; Zhu et al., 2010), and remnants of ca. 820-810 continental flood basalts represented by the 820-810 Ma Bikou tholeiites (#4 in Fig.

1B; Wang et al., 2008) and the ca. 820 Ma Tiechuanshan tholeiites (#3 in Fig. 1B; Ling et al., 2003). Also consistent with the involvement of a mantle plume is the kilometer-scale lithospheric doming prior to the emplacement of the Guibei LIP (Li et al., 1999).

If the interpreted Guibei LIP is correct, the bulk of it must have been eroded away due to rapid continental domal and unroofing and young geological processes, with only patchy remnants of the ca. 825–800 Ma basalts preserved inside rift basin remnants (Li at al., 1999, 2008b; Wang et al., 2008, 2010a). As basalts weather five to ten times more rapidly than granites (Desert et al., 2003), detrital input from the CFBs could have played a major role in the geochemical and isotopic characteristics of the Neoproterozoic rift successions, as discussed in section 5.3. Indeed, Figure 10 shows that all but one of the studied sedimentary specimens plot in the field of the Bikou CFBs, tholeiitic remnants of the ca. 820–810 Ma Guibei LIP (Wang et al., 2008; Ernest et al., 2008; Li et al., 2008b; Wang et al., 2010b; see recent update at http://www.largeigneousprovinces.org/09may.html). Furthermore, the studied samples define a linear array on the Hf-Nd isotopic space that passes through the average composition of the Bikou CFBs (Fig. 10).This suggests that the high proportions of mafic materials in the source provenance may indeed reflect a large-scale erosion of the Neoproterozoic CFBs in the South China Block.

Another possible interpretation is that the juvenile materials originated from the ca. 1.3–0.9 Ga Sibao-aged arc igneous rocks (, Li et al., 2002b, 2007c, 2008b, 2009a, b; Ye et al., 2007). However, the following lines of evidence argue against this possibility. First, although igneous rocks of arc-origin may have elevated εNd(t) and εHf(t) values, they generally have low Cr, Co, Sc, V and Ni abundances (e.g., Taylor and McLennan, 1985). Thus, whereas input from juvenile materials of arc-origin into the Neoproterozoic clastic sedimentary rocks could explain the somewhat elevated Nd isotope ratios, it could not account for the correlations of Cr, Sc, V, and Th/Sc with MgO (Fig. 4A, D-F) and the trends presented in Figure 9. Second, recently reported *in situ* zircon Hf-O isotope and U-Pb dating results suggest that any contribution from the Sibao-aged arc igneous rocks to the sedimentary rocks in the Nanhua Rift Basin is insignificant (Wang et al., 2011a, b). Hf isotopes of dated zircon grains (samples 08SC07, 08SC11, 08SC31 and 08SC74) showed no zircon grain plotting within the growth curves between new continental crust and depleted mantle at ca. 1.3–0.9 Ga (figure 11a of Wang et al., 2011a), and that zircon grains with positive εHf(t) values (n = 530, figure 10a of Wang et al., 2011a) peak at 0.9–0.7 Ga. Oxygen isotopes of dated zircon grains (samples 08SC07, 08SC11, 08SC31 and 08SC15) showed that zircon grains with mantle-like $\delta^{18}O$ values (5.3 ± 0.8 ‰) also peak at ca. 0.9–0.7 Ga (figure 3 of Wang et al., 2011b). Furthermore, zircon U-Pb dating shows that zircon grains with the ages of ca. 1.3–0.9 Ga are insignificant (figure 10 of Wang et al., 2011a).

The Adelaide Rift Complex also has a well-preserved Neoproterozoic rift succession, starting at ca. 820 Ma with basalts, clastic and glaciogenic sediments, and carbonates (e.g., Preiss, 2000). The associated Willouran LIP in southern-central Australia is dominated by tholeiitic mafic dykes (the Gairdner dykes), flood basalts (the Wooltana basalts), and mafic intrusions (Wang et al., 2010b and references therein). If Australia was next to South China as proposed by Li et al. (1995, 2008b), the Neoproterozoic LIPs and rift successions of the two continents are expected to share similar characteristics. Geochemical and geochronological evidence showed that the Guibei LIP in South China and Willouran LIP in southern-central Australia have similar source regions and comparable age distributions, suggesting that the two LIPs were likely cogenetic and could have been parts of a once contiguous LIP that was dismembered during the breakup of Rodinian (Wang et al., 2010b). Fine-grained siliciclastic pre-Sturtian rocks of southern-central Australia (the Adelaide Rift Complex, and the Amadeus and Officer basins) documents a significant positive excursion in εNd(t) values, from -12 to -4 (Fig. 8). Barovich and Foden (2000) interpreted this anomaly to represent the extrusion and weathering of ca. 825-800 Ma CFBs as part of the Willouran LIP, presumably related to rifting of the eastern margin of the Australia craton during Rodinian fragmentation (Li et al., 2003b and 2008b). A roughly coeval positive excursion is found in Nanhua Rift Basin (Fig. 8). Furthermore, Neoproterozoic sedimentary rocks from the two continents show similar trends in εNd(t) when plotted against trace elemental ratios of La/Sc, La/V, La/Cr, La/Co and La/Ni (Fig. 9). These trends pass through a common basaltic end-member, which is similar to the average value of ca. 825-810 Ma Bikou-Tiechuanshan CFBs in the South China Block. This suggests that the Neoproterozoic rift sedimentary rocks from the two continents could indeed have recorded a similar CFB provenance. Thus, isotope and chemical data from fined-grained sedimentary rocks present another means of tracing the extents of eroded CFBs and testing or establishing conjugate continental margins in supercontinent reconstructions (Halverson et al., 2010).

Therefore, although the position of the South China Block in the Rodinia supercontinent is still controversial (e.g., Li et al., 1995, 1999, 2002b, 2003a, b, 2008b; Zhou et al., 2002b, 2006; Wang et al., 2007a, b; Yu et al., 2010), this study favors the position of the South China Block being adjacent to eastern Australia in Rodinian (Li et al., 1995, 1999, 2003b, 2008b) and argues against the alternative model proposed by Zhou et al. (2002b, 2006).

6. Conclusions

Geochemical and isotopic features of Neoproterozoic sedimentary rocks in the Nanhua Rift Basin of South China require large proportional input of mafic rocks in their source provenance, most likely eroded Neoproterozoic CFBs. Although preserved only as feeder dykes and isolated volcanic rocks today, the sedimentary record support the once existence of a Neoproterozoic continental flood basalt province in South China. The similarities in geochemical and isotopic signatures between the Neoproterozoic rift sediments in both South China and Australia, along with their similar magmatic and rifting history, suggest that the two continents may have been adjacent to each other in the Rodinia supercontinent and shared a single continental flood basalt province during the breakup of Rodinia.

Acknowledgements

We thank Bin He and Galen Halverson and editor Andrew Kerr for their constructive and helpful reviews. We are grateful to J. Li, Y.H. Yang, X.L. Tu, G.Q.

Hu and W. Zeng for assistance in geochemical analyses. This work was supported by the National Natural Science foundation of China (grants 40773007, 40803010 and 40973044) and the Australian Research Council (ARC) Discovery Project grant (DP0770228). This is TIGeR (The Institute of Geoscience Research, Curtin University) publication No. xx.

References

Barovich, K.M. and Foden, J., 2000. A Neoproterozoic flood basalt province in southern-central Australia: geochemical and Nd isotope evidence from basin fill. Precambrian Research 100, 213-234.

Barth, M.G., McDonough, W.F. and Rudnick, R.L., 2000. Tracking the budget of Nb and Ta in the continental crust. Chemical Geology 165, 197-213.

Bayon, G., Burton, K.W., Soulet, G., Vigier, N., Dennielou, B., Etoubleau, J., Ponzevera, E., German, C.R. and Nesbitt, R.W., 2009. Hf and Nd isotopes in marine sediments: Constraints on global silicate weathering. Earth and Planetary Science Letters 277, 318-326

Chen, J., Zhou, T., Xing, F., Xu, X. and Foland, K.A., 1989. Provenances of low-grade metamorphic and sedimentary rocks from South Anhui Province: evidence of Nd isotope compositions. Chinese Science Bulletin 34, 1572-1574 (in Chinese).

Chen, J. and Jahn, B.M., 1998. Crustal evolution of southeastern China: Nd and Sr isotopic evidence. Tectonophysics 284, 101-133.

Condie, K.C., 1993. Chemical composition and evolution of the upper continental crust: contrasting results from surface samples and shales. Chemical Geology 104, 1–37.

Cox, R., Lowe, D.R. and Cullers, R.L., 1995. The influence of sediment recycling and basement composition on evolution of mudrock chemistry in the southwestern United States. Geochimica et Cosmochimica Acta 59, 2919-2940.

Cullers, R.L., Basu, A. and Suttner, L., 1988. Geochemical signature of provenance in sand-size material in soils and stream sediments near the Tobacco Root batholith, Montana, USA. Chemical Geology 70, 335-348.

Dessert, C., Dupré, B., Gaillardet, J., François, L. M. and Allègre, C. J., 2003. Basalt weathering laws and the impact of basalt weathering on the global carbon cycle. Chemical Geology 202, 257-273.

Ernst, R.E., Wingate, M.T.D., Buchan, K.L. and Li, Z.X., 2008. Global record of 1600-700 Ma Large Igneous Provinces (LIPs): Implications for the reconstruction of the proposed Nuna (Columbia) and Rodinia supercontinents. Precambrian Research 160, 159-178.

Fedo, C.M., Nesbitt, H.W. and Young, G.M., 1995. Unraveling the effects of potassium metasomatism in sedimentary rocks and paleosols, with implications for paleoweathering conditions and provenance. Geology 23, 921-924.

Gao, L.Z., Dai, C.G., Liu, Y., Wang, M., Wang, X.H., Chen, J.S., Ding, X.Z., 2010a. Zircon SHRIMP U-Pb dating of the tuffaceous bed of Xiajiang Group in

Guizhou Province and its stratigraphic implications. Geol. China 37, 1071-1080 (Chinese with English abstract).

Gao, L.Z., Dai, C.G., Liu, Y., Wang, M., Wang, X.H., Chen, J.S., Ding, X.Z., Zhang, C.H., Gao, C.Q., Liu, J.H., 2010b. Zircon SHRIMP U-Pb dating of tuff bed of the Sibao Group in Southeastern Guizhou-northern Guangxi area, China and its stratigraphic implication. Geol. Bull. China 29, 1259-1267 (Chinese with English abstract).

Gao, S., Ling, W., Qiu, Y. and Lian, Z., Hartmann, G. and Simon, K., 1999. Contrasting geochemical and Sm-Nd isotopic compositions of Archean metasediments from the Kongling high-grade terrain of the Yangtze craton: evidence for cratonic evolution and redistribution of REE during crustal anatexis. Geochimica et Cosmochimica Acta 63, 2071-2088.

Goto, A., Tatsumi, Y., 1996. Quantitative analyses of rock samples by an x-ray fluorescence spectrometer (II). Rigaku Journal 13, 20–39.

Gu, X.X., Liu, J.M., Zheng, M.H., Tang, J.X. and Qi, L., 2002. Provenance and tectonic setting of the Proterozoic turbidites in Hunan, South China: geochemical evidence. Journal of Sedimentary Research 72, 393-407.

Halverson, G. P., Wade, B. P., Hurtgen, M. T. and Barovich, K. M., 2010. Neoproterozoic chemostratigraphy. Precambrian Research 182, 337-350. Herron, M.M., 1988. Geochemical classification of terrigenous sands and shales from core or log data. Journal of Sedimentary Research 58, 820-829.

Hill, R., Campbell, I.H., Davies, G.F. and Griffiths, R.W., 1992. Mantle plumes and continental tectonics. Science 256, 186-193.

Li, W.X., Li, X.H. and Li, Z.X., 2010a. Ca. 850 Ma bimodal volcanic rocks in northeastern Jiangxi, South China: initial extension during the breakup of Rodinia. American Journal of Science 310, 951-980.

Li, W.X., Li, X.H. and Li, Z.X., 2008a. Middle Neoproterozoic syn-rifting volcanic rocks in Guangfeng, South China: petrogenesis and tectonic significance. Geological Magazine 145, 475-489.

Li, W.X., Li, X.H. and Li, Z.X., 2005. Neoproterozoic bimodal magmatism in the Cathaysia Block of South China and its tectonic significance. Precambrian Research 136, 51-66.

Li, X.H., Li, W.-X., Li, Q.-L., Wang, X.-C., Liu, Y. and Yang, Y.-H., 2010b. Petrogenesis and tectonic significance of the ~850 Ma Gangbian alkaline complex in South China: Evidence from in situ zircon U-Pb dating, Hf-O isotopes and whole-rock geochemistry. Lithos 114, 1-15.

Li, X.H., Li, W.X., Li, Z.X., Lo, C.H., Wang, J., Ye, M.F. and Yang, Y.H., 2009a. Amalgamation between the Yangtze and Cathaysia Blocks in South China: Constraints from SHRIMP U-Pb zircon ages, geochemistry and Nd-Hf isotopes of the Shuangxiwu volcanic rocks. Precambrian Research 174, 117–128.

Li, X.H., Liu, Y., Yang, Y.H., Chen, F.K., Tu, X.L. and Qi, C.S., 2007a. Rapid separation of Lu-Hf and Sm-Nd from a single rock dissolution and precise measurement of Hf-Nd isotopic ratios for national rock standards. Acta

Petrologica Sinica 23, 221-226 (in Chinese with English abstract).

Li, X.H., Li, Z.X., Sinclair, J.A., Li, W.X. and Carter, G., 2007b. Reply to the comment by Zhou et al. on: "Revisiting the "Yanbian Terrane": Implications for Neoproterozoic tectonic evolution of the western Yangtze Block, South China". Precambrian Research 155, 318-323.

Li, X.H., Li, Z.X., Sinclair, J.A., Li, W.X. and Carter, G., 2006. Revisiting the "Yanbian Terrane": implications for Neoproterozoic tectonic evolution of the western Yangtze Block, South China. Precambrian Research 151, 14-30.

Li, X.H., Liu, D.Y., Sun, M., Li, W.X., Liang, X.R. and Liu, Y., 2004. Precise Sm–Nd and U–Pb isotopic dating of the super-giant Shizhuyuan polymetallic deposit and its host granite, Southeast China. Geological Magazine 141, 225-231.

Li, X.H., Li, Z.X., Ge, W.C., Zhou, H.W., Li, W.X., Liu, Y. and Wingate, M.T.D., 2003a. Neoproterozoic granitoids in South China: crustal melting above a mantle plume at ca. 825 Ma? Precambrian Research 122, 45-83.

Li, X.H., Li, Z.X., Zhou, H., Liu, Y. and Kinny, P.D., 2002a. U-Pb zircon geochronology, geochemistry and Nd isotopic study of Neoproterozoic bimodal volcanic rocks in the Kangdian Rift of South China: implications for the initial rifting of Rodinia. Precambrian Research 113, 135-154.

Li, X.H., 1999. U–Pb zircon ages of granites from the southern margin of Yangtze Block and the timing of Neoproterozoic Jinning Orogeny in SE China: termination of Rodinia assembly? Precambrian Research 97, 43–57.

Li, X.H., 1997. Geochemistry of the Longsheng ophilite from the southern margin of

Yangtze Craton, SE China. Geochemical Journal 31, 323–337.

Li, X.H. and McCulloch, M.T., 1996. Secular variation in the Nd isotopic composition of Neoproterozoic sediments from the southern margin of the Yangtze Block: evidence for a Proterozoic continental collision in southeast China. Precambrian Research 76, 67-76.

Li, Z.X., Li, X.H. and Wang, X.C., 2009b. The South China piece in the Rodinian puzzle: A reply to the comment by Munteanu and Wilson. Precambrian Research 171, 77-79.

Li, Z.X. and Zhong, S., 2009. Supercontinent-superplume coupling, true polar wander and plume mobility: Plate dominance in whole-mantle tectonics. Physics of the Earth and Planetary Interiors 176, 143-156.

Li, Z.X., Bogdanova, S.V., Collins, A.S., Davidson, A., De Waele, B., Ernst, R.E., Fitzsimons, I.C.W., Fuck, R.A., Gladkochub, D.P., Jacobs, J., Karlstrom, K.E., Lu, S., Natapov, L.M., Pease, V., Pisarevsky, S.A., Thrane, K. and Vernikovsky, V., 2008b. Assembly, configuration, and break-up history of Rodinia: A synthesis. Precambrian Research 160, 179-210.

Li, Z.X., Li, X.H., Zhou, H.W., and Kinny, P.D., 2002b. Grenvillian continental collision in South China: New SHRIMP U-Pb zircon results and implications for the configuration of Rodinia. Geology 30, 163-166.

Li, Z.X., Li, X.H., Kinny, P.D., Wang, J., Zhang, S. and Zhou, H., 2003b. Geochronology of Neoproterozoic syn-rift magmatism in the Yangtze Craton, South China and correlations with other continents: evidence for a mantle superplume that broke up Rodinia. Precambrian Research 122, 85-109.

Li, Z.X., Li, X.H., Kinny, P.D. and Wang, J., 1999. The breakup of Rodinia: did it start with a mantle plume beneath South China? Earth and Planetary Science Letters 173, 171-181.

Li, Z.X., Wartho, J.A., Occhipinti, S., Zhang, C.L., Li, X.H., Wang, J. and Bao, C.M., 2007c. Early history of the eastern Sibao Orogen (South China) during the assembly of Rodinia: new mica $^{40}Ar/^{39}Ar$ dating and SHRIMP U－Pb detrital zircon provenance constraints. Precambrian Research 159, 79-94.

Li, Z.X., Zhang, L. and Powell, C.M., 1995. South China in Rodinia: part of the missing link between Australia–East Antarctica and Laurentia? Geology 23, 407-410.

Ling, H., Shen, W., Zhang, B., Liu, J., Yang, J. and Tao, X., 1992. Nd isotopic composition and material source of Pre- and Post-Sinian sedimentary rocks in Xiushui Area, Jiangxi Province. Chinese Journal of Geochemistry 11, 80-87.

Ling, W., Gao, S., Zhang, B., Li, H., Liu and Y. Cheng, J., 2003. Neoproterozoic tectonic evolution of the northwestern Yangtze craton, South China: implications for amalgamation and break-up of the Rodinia Supercontinent. Precambrian Research 122, 111-140.

Liu, Y., Liu, H.C., Li, X.H., 1996. Simultaneous and precise determination of 40 trace elements in rock samples using ICP-MS. Geochimica 25, 552-558 (in Chinese with an English abstract).

Ma, J.L., Wei, G.J., Xu, Y.G., Long, W.G., Sun, W.D., 2007. Mobilization and re-distribution of major and trace elements during extreme weathering of basalt in Hainan Island, South China. Geochimica Et Cosmochimica Acta 71, 3223-3237.

McLennan, S.M., Taylor, S.R., McCulloch, M.T. and Maynard, J.B., 1990. Geochemical and Nd－Sr isotopic composition of deep-sea turbidites: Crustal evolution and plate tectonic associations. Geochimica et Cosmochimica Acta 54, 2015－2050.

Nesbitt, H.W., MacRae, N.D. and Kronberg, B.I., 1990. Amazon deep sea fan muds: light REE enriched products of extreme chemical weathering. Earth and Planetary Science Letters 100, 118– 123.

Nesbitt, H.W., and Young, G.M., 1984. Prediction of some weathering trends of plutonic and volcanic rocks based on thermodynamic and kinetic considerations. Geochimica et Cosmochimica Acta 48, 1523–1534.

Preiss, W.V., 2000. The Adelaide Geosyncline of South Australia and its significance in Neoproterozoic continental reconstruction. Precambrian Research 100, 21-63.

Rudnick R.L. and Gao S., 2003. Composition of the continental crust. In: Holland, H.D. and Turekian, K.K (Eds), The Crust, Treatise on Geochemistry, vol.3, pp.1-64.

Saunders, A.D., Tarney, J., Kerr, A.C. and Kent, R.W., 1996. The formation and fate of large oceanic igneous provinces. Lithos 37, 81-95.

Shen, W.Z., Ling, H.F., Shu, L.S., Zhang, R.F. and Xiang, L., 2009. Sm-Nd isotope compositions of Cambrian-Ordovician strata at the Jianggangshan area in Jiangxi Province: Tectonic implications. Chinese Science Bulletin 54, 1750-1758.

Singh, P., 2009. Major, trace and REE geochemistry of the Ganga River sediments: Influence of provenance and sedimentary processes. Chemical Geology 266, 242-255.

Sun, S.S., McDonough, W.F., 1989. Chemical and isotopic systematics of oceanic basalts: implications for mantle composition and processes. In: A.D. Saunders and M.J. Norry (Eds.), Magmatism in the Ocean Basins. Geological Society, London, Special Publications 42, pp313-345.

Tanaka, T., Togashi, S., Kamioka, H., Amakawa, H., Kagami, H., Hamamoto, T., Yuhara, M., Orihashi, Y., Yoneda, S. and Shimizu, H., 2000. JNdi-1: a neodymium isotopic reference in consistency with LaJolla neodymium. Chemical Geology 168, 279-281.

Taylor, S.R. and McLennan, S.M., 1985. The Continental Crust: its Composition and Evolution. Blackwell, Oxford, 312 pp.

Turner, S., Foden, J., Sandiford, M., Bruce, D., 1993. Sm-Nd isotopic evidence for the provenance of sediments from the Adelaide Fold Belt and southeastern Australia with implications for episodic crustal addition. Geochimica Et Cosmochimica Acta 57, 1837-1856.

Ugidos, J.M., Valladares, M.I., Recio, C., Rogers, G., Fallick, A.E. and Stephens, W.E. 1997. Provenance of Upper Precambrian–Lower Cambrian shales in the

Central Iberian Zone, Spain: evidence from a chemical and isotopic study. Chemical Geology 136, 55–70.

Vervoort, J.D., Patchett, P.J., Blichert-Toft, J. and Albarede, F., 1999. Relationships between Lu-Hf and Sm-Nd isotopic systems in the global sedimentary system. Earth and Planetary Science Letters 168, 79-99.

Wang, J., Zeng, Z.G., Chen, W.X., Wang, Z.J., Xiong, G.Q. and Wang, X.H., 2006. The Neoproterozoic rift systems in southern China: New evidence for the sedimentary onlap and its initial age. Sedimentary Geology and Tethyan Geology 26, 1-8 (in Chinese with English abstract).

Wang, J. and Li, Z. X., 2003. History of Neoproterozoic rift basins in South China: implications for Rodinia break-up. Precambrian Research 122, 141-158.

Wang, J., Li, X. H., Duan, T.Z., Liu, D.Y., Song, B., Li, Z.X. and Gao, Y.H., 2003. Zircon SHRIMP U-Pb dating for the Cangshuipu volcanic rocks and its implications for the lower boundary age of the Nanhua strata in South China. Chinese Science Bulletin 48, 1663-1669.

Wang, Q., Wyman, D.A., Li, Z.X., Bao, Z.W., Zhao, Z.H., Wang, Y.X., Jian, P., Yang, Y.H. and Chen, L.L., 2010a. Petrology, geochronology and geochemistry of ca. 780 Ma A-type granites in South China: Petrogenesis and implications for crustal growth during the breakup of the supercontinent Rodinia. Precambrian Research 178, 185-208.

Wang, X.C., Li, X.H., Li, Z.X., Li, Q.L., Tang, G.Q., Gao, Y.Y., Zhang, Q.R., Liu, Y, 2011a. Episodic Precambrian crust growth: Evidence from U-Pb ages and

Hf-O isotopes of zircon in the Nanhua Basin, central South China. Precambrian Research doi:10.1016/j.precamres.2011.06.001.

Wang, X.C., Li, Z.X., Li, X.H., Li, Q.L., Tang, G.Q., Zhang, Q.R., Liu, Y., 2011b. Nonglaciation origin for low $\delta^{18}O$ Neoproterozoic magmas in the South China Block: Evidence from new in-situ oxygen isotope analyses using SIMS. Geology 39, 735-738.Wang, X.C., Li, X.H., Li, Z.X. and Liu, Y., 2010b. The Willouran Basic Province of South Australia: its relation to the Guibei Large Igneous Province in South China and the breakup of Rodinia. Lithos 119, 569-584.

Wang, X.C., Li, X.H., Li, W.X. and Li, Z.X., 2009. Variable involvements of mantle plumes in the genesis of mid-Neoproterozoic basaltic rocks in South China: A review. Gondwana Research 15, 381-395.

Wang, X.C., Li, X.H., Li, W.X., Li, Z.X., Liu, Y., Yang, Y.H., Liang, X., R. and Tu, X.L., 2008. The Bikou basalts in northwestern Yangtze Block, South China: Remains of 820-810 Ma continental flood basalts? Geological Society of American Bulletin 120, 1478-1492.

Wang, X.C., Li, X.H., Li, W.X. and Li, Z.X., 2007a. Ca. 825 Ma komatiitic basalts in South China: First evidence for >1500 ^{o}C mantle melts by a Rodinian mantle plume. Geology 35, 1103-1106.

Wang, X.L., Zhou, J.C., Griffin, W.L., Wang, R.C., Qiu, J.S., O'Reilly, S.Y., Xu, X., Liu, X.-M. and Zhang, G.L., 2007b. Detrital zircon geochronology of Precambrian basement sequences in the Jiangnan orogen: Dating the assembly of the Yangtze and Cathaysia Blocks. Precambrian Research 159, 117-131.

Wu, F.Y., Sun, J.P. and Zhang, X.Z., 1998. The Nd isotopic evidence for late Paleozoic oceanic crust in southern margin of Yangtze Block. Acta Petrologica Sinica 14, 22-33 (in Chinese with English abstract).

Ye, M.F., Li, X.H., Li, W.X., Liu, Y., Li, Z.X., 2007. SHRIMP zircon U–Pb geochronological and whole-rock geochemical evidence for an early Neoproterozoic Sibaoan magmatic arc along the southeastern margin of the Yangtze Block. Gondwana Research 12: 144-156.

Yin, C.Y., Liu, Y.Q., Gao, L.Z., Tang, F. and Liu, P.J., 2007. Phosphatized Biota in Early Sinian (Edicaran): Weng An Biota and its Environment. Beijing, Geological Publishing House, pp.1-126.

Yu, J.H., O'Reilly, S.Y., Wang, L.J., Griffin, W.L., Zhou, M.F., Zhang, M. and Su, L.S., 2010. Components and episodic growth of Precambrian crust in the Cathaysia Block, South China: Evidence from U–Pb ages and Hf isotopes of zircons in Neoproterozoic sediments. Precambrian Research 181, 97-114.

Zhang, C.H., Liu, Y.M., Shi, X.Y., Gao, L.Z. and Zhang, C., 2009. Sedimentological features of the Xiajiang Group and their constraints on the Neoproterozoic tectonic evolution of South China. Acta Geoscientica Sinica 30, 495-504 (Chinese with English abstract).

Zhang, Q.R., Li, X.H., Feng, L.J., Huang, J. and Song, B., 2008a. A new age constraint on the onset of the Neoproterozoic glaciations in the Yangtze Platform, South China. Journal of Geology 116, 423-429.

Zhang, S.H., Jiang, G.Q., Dong, J., Han, Y.G. and Wu, H.C., 2008b. New SHRIMP U-Pb age from the Wuqiangxi Formation of Banxi Group: Implications for rifting and stratigraphic erosion associated with the early Cryogenian (Sturtian) glaciation in South China. Science in China Series D: Earth Sciences 51, 1537-1544.

Zhou, C., Tucker, R., Xiao, S., Peng, Z., Yuan, X. and Chen, Z., 2004. New constraints on the ages of Neoproterozoic glaciations in south China. Geology 32, 437-440.

Zhou, H., Li, X.H., Wang, H., Li, J. and Li, H., 2002a. U–Pb zircon geochronology of basic volcanic rocks within the Yingyangguan Group in Hezhou, Guangxi, and its tectonic implications. Geological Review 48 (Suppl.), 22–25 (in Chinese with English abstract).

Zhou, J., Li, X.H., Ge, W. and Li, Z.X., 2007. Age and origin of middle Neoproterozoic mafic magmatism in southern Yangtze Block and relevance to the break-up of Rodinia. Gondwana Research 12, 184-197.

Zhou, J.-C., Wang, X.-L., Qiu, J.-S., 2009. Geochronology of Neoproterozoic mafic rocks and sandstones from northeastern Guizhou, South China: Coeval arc magmatism and sedimentation. Precambrian Research 170, 27-42.

Zhou, M.F., Yan, D. P., Kennedy, A.K., Li, Y. and Ding, J., 2002b. SHRIMP U-Pb zircon geochronological and geochemical evidence for Neoproterozoic arc-magmatism along the western margin of the Yangtze Block, South China. Earth and Planetary Science Letters 196, 51-67.

Zhou, M.F., Yan, D.-P., Wang, C.L., Qi, L. and Kennedy, A., 2006. Subduction-related origin of the 750Ma Xuelongbao adakitic complex (Sichuan Province, China): Implications for the tectonic setting of the giant Neoproterozoic magmatic event in South China. Earth and Planetary Science Letters 248, 286-300.

Zhu, W.G., Li, X.H., Zhong, H., Wang, X.C., He, D.F., Bai, Z.J., Liu, F., 2010. The Tongde Picritic Dikes in the Western Yangtze Block: Evidence for ca. 800-Ma mantle plume magmatism in South China during the breakup of Rodinia: The Journal of Geology 118, 509-522.

Zhu, W.G., Zhong, H., Li, X.H., Liu, B.G., Deng, H.L. and Qin, Y., 2007. ^{40}Ar-^{39}Ar age, geochemistry and Sr-Nd-Pb isotopes of the Neoproterozoic Lengshuiqing Cu-Ni sulfide-bearing mafic-ultramafic complex, SW China. Precambrian Research 155, 98-124.

Figure captions

Fig. 1 (A) Proposed ca. 825 Ma South China mantle plume model for the genesis of the Guibei and Willouran large igneous provinces (LIPs), and positions of the Nanhua, Kangdian, Bikou–Hannan, and Adelaide rift systems in the Rodinia reconstruction of Li et al. (1999, 2003b, and 2008b). Geochemical evidence shows that the two LIPs could have been parts of a once contiguous LIP, which was dismembered during the breakup of Rodinia (Wang et al., 2010b). (B) Schematic map of Precambrian South China emphasizing the three Neoproterozoic continental rift systems (after Li et al., 1999; Wang and Li, 2003; Wang et al., 2011a, b). (C) A simplified geological map showing the outcrop distribution of the Xiajiang Group (Gr) (Guizhou province), Danzhou Group (Guangxi province) and Banxi Group (Hunan province). Open circles in (B) represent locations of well-dated Neoproterozoic basaltic rocks in the South China Block: 1 = 782 ± 10 Ma Bijigou gabbro; 2 = Wangjiashan 819 ± 10 Ma diorite and 808 ± 14 Ma gabbro; 3 = 817 ± 5 Ma Tiechuanshan tholeiites; 4 = 821 ± 7 Ma to 811 ± 12 Ma Bikou tholeiites; 5 = 839 ± 9 Ma Dongjiaheba gabbro; 6 = 780 to 760 Ma mafic dyke swarm; 7 = 753 ± 11 Ma and 753 ± 12 shaba gabbro; 8 = 803 ± 12 Ma Suxiong alkalic basalt; 9 = 821 ± 3 Ma Lengshuiqing mafic-ultramafic complex with Cu-Ni-PGE mineralisation; 10 = 796 ± 5 Ma Tongde picritic dike (Zhu et al., 2010); 11 = 830-820 Ma mafic dyke swarm, gabbros and mafic-ultramafic complex; 12 = 822 ± 15 Ma Fanjinshan basalts; 13 = Longsheng gabbro 761 ± 8 Ma; 14 = 768 ± 28 Ma Guzhang dolerite; 15 = 832 ± 10 Ma Aikou mafic-ultramafic dyke swarm; 16 = 823 ± 6 Yiyang anhydrous high-Mg basalts; 17 = 818 ± 9 Ma Mamianshan basalt; 18 = 827 ±

14 Ma Guangfeng basalts; 19 = 755 ± 2 Ma Wudang mafic dyke swarm. Source of quoted ages are listed in appendix table 1 of Wang et al. (2011a). The dashed line in Figure 1B outlines the likely regional extent of the Guibei large igneous province (LIP). It has an age of ca. 825–810 Ma and was interpreted to be produced by a mantle plume linked to the breakup of the supercontinent Rodinia (Li et al., 2008, and a recent update at http://www. largeigneousprovinces.org/09may.html).

Fig. 2 Synthesized regional stratigraphic columns of the Neoproterozoic rift successions in South China (modified after Wang and Li, 2003). Sources for the quoted ages: A1, A11 – Gao et al., 2010b; A2, A3 and A10 – Wang et al., 2006; A4, A5, A6– Gao et al., 2010a; A7 – Zhou et al., 2004; A8 – Li et al., 1999 ; A9 – Li, 1999 ; A11 – Zhou et al., 2007; A13 – Zhang et al., 2009; A14 – Wang et al., 2003, A15–Zhang et al., 2008b, A16–Zhang et al., 2008a . Gr = Group; Fm = Formation. The detrital zircons from sandstone sample 08SC74 give a youngest age population of ca. 730 Ma (Wang et al., 2011a).

Fig. 3 Plots of major and trace elements versus Al_2O_3 for the Nanhua Rift sedimentary samples. The light-shaded field represents the composition of synchronous sediments from the Adelaide Rift Complex (Barovich and Foden, 2000).

Fig. 4 Plot of transition trace elements and Th/Sc ratios versus MgO. The light-shaded field represents the composition of synchronous sediments from the Adelaide Rift

Complex (Barovich and Foden, 2000).

Fig. 5. Chemical classification of sedimentary rocks from Nanhua Rift basin using log (SiO_2/Al_2O_3) vs. log (Fe_2O_3/K_2O) diagram (Herron, 1988).

Fig. 6 Chondrite-normalized REE diagrams for (A) pelites; (B) siltstone/pelitic siltstone; (C) tuffs/tuffaceous siltstones; and (D) sandstones/tuffaceous sandstones from the Nanhua Rift (Appendix A). The patterns are similar to that of the upper continental crust and typical post-Archean shales (PAAS: Post-Archean average Australia shale; Taylor and McLennan, 1985), with LREE enrichment, flat HREE, but intermediate to negligible negative Eu anomalies. Chondrite-normalizing factors are from Sun and McDonough (1989). Data for the average of 825–810 Ma Bikou continental flood basalts (CFBs) are from Wang et al. (2008). Grey field indicates the range of ca. 825-800 Ma basaltic rocks in South China (Wang et al., 2009 and references therein). UUC: upper continental crust (Rudnick and Gao, 2003). PAAS: post-Archaean Australia shale (Taylor and McLennan, 1985).

Fig. 7 Histogram of Nd isotopes for (A) ca. 825 Ma granites in northern Guangxi; (B) middle-upper part (ca. 820–635 Ma) of Cryogenian sedimentary rocks; (C) ca. 825–750 Ma basaltic rocks. The data for ca. 830-820 Ma granites in northern Guangxi are after Li et al. (2003a). The data for ca. 825–750 Ma basaltic rocks are after Li et al. (2002a, 2005, 2008a), Zhou et al. (2002a, 2007, 2009), Zhu et al. (2007), and Wang et al. (2008, 2009 and references therein).

Fig. 8 Plot of εNd(t) versus stratigraphic ages of the sedimentary samples in South China and Australia. Data for the Proterozoic/Archean basement are from the Kongling area (Gao et al., 1999). Data for the Nanhua Rift is from this study. Other South China data (open circles) is from Chen et al. (1989), Ling et al. (1992), Li and McCulloch (1996), Chen and Jahn (1998), Wu et al. (1998) and Shen et al. (2009). Australian data (the Adelaide Rift Complex, and the Amadeus and Officer basins) is from a summary of Halverson et al. (2010).

Fig. 9 Plots of εNd(t) versus (A) La/Sc, (B) La/V, (C) La/Co, (D)La/Cr, and (E) La/Ni of sedimentary rocks in the Nanhua Rift compared with that of synchronous sedimentary rocks in the Adelaide Rift Complex, Australia. Data for sediments in the Adelaide Rift Complex are from Barovich and Foden (2000) and Turner et al. (1993). Solid lines represent the mixing trend between the mafic and granitic end-members. The field of basaltic rocks is defined by the ca. 820-810 Bikou tholeiites (Wang et al., 2008), 817 ± 5 Ma Tiechuanshan tholeiites (Ling et al., 2003), 803 ± 12 Ma Suxiong alkalic basalt (Li et al., 2002a), 822 ± 15 Ma Fanjinshan basalts (Zhou et al., 2009), 823 ± 6 Yiyang anhydrous high-Mg basalts (Wang et al., 2007a), 818 ± 9 Ma Mamianshan basalt (Li et al., 2005), and 827 ± 14 Ma Guangfeng basalts (Li et al., 2008a). The field of granites is defined by ca.830–820 Ma granites from northern Guangxi (Li et al., 2003a). Each dot on the lines represents a 10% increment of basaltic component. Dashed lines are regression lines for the sedimentary rocks from

Adelaide Rift Complex. The basaltic end-member is estimated using the average of the ca. 825–750 Ma basaltic rocks (Wang et al., 2009 and references therein) with La = 29 ppm, Ni = 84 ppm, Co = 43 ppm, Cr = 154 ppm, V = 228 ppm, Sc = 35 ppm, εNd(t) = +2.8. These values are similar to the average values of the Bikou-Tiechuanshan CFBs (La = 25 ppm, Ni = 93 ppm, Co = 53 ppm, Cr = 200 ppm, V = 250 ppm, Sc = 30 ppm, εNd(t) = 3.2; Ling et al., 2003; Wang et al., 2008). The granitic end-member has εNd(t) = -6, Ni = 12 ppm, Co = 6 ppm, Cr = 30 ppm, V = 36 ppm, and Sc = 5 ppm. The Nd isotope composition for the granitic end-member is estimated using the average of the ca. 830–820 Ma granites in northern Guangxi (Fig. 1C; Li et al., 2003a). Parameters r_1 and r_2 represent the correlation coefficients for sedimentary rocks from the Nanhua Rift and the Adelaide Rift Complex, respectively.

Fig. 10 εHf(t) versus εNd(t) plots of samples from the Nanhua Rift compared to the ca. 825-810 Ma Bikou continental flood basalts (CFBs; Wang et al., 2008), 'terrestrial array' (εHf = 1.36εNd+ 2.95; Vervoort et al., 1999), 'seawater array' defined by marine Fe-Mn precipitates (εHf = 0.39εNd+ 6.2; Bayon et al., 2009), 'zircon-free sediment array' defined by fine-grained sediments (εHf = 0.91εNd+ 3.10; Bayon et al., 2009), and 'zircon-bearing sediment array' defined by coarse-grained sediments (εHf = 1.80εNd+ 2.95; Bayon et al., 2009). Filled star: the average of the Bikou continental flood basalts (εNd(t) = +3 and εHf(t) = +7; Wang et al., 2008); Open star: the average of the Wooltana continental flood basalts (εNd(t) = +3 and εHf(t) = +8; Wang et al., 2010a).

Fig. 11 (A) Ternary plot of molecular proportions Al_2O_3-(Na_2O + CaO*)-K_2O (Fedo et al., 1995) for fine-grained sedimentary rocks from the Nanhua Rift. (B) Chemical weathering, K-metasomatism and retrograde alteration trends of the Nanhua Rift sediments shown on a A-CN-K ternary diagram. Dashed lines in (A) are reconstruction for K-metasomatism of the Nanhua Rift sediments is according to the method proposed by Fedo et al. (1995). K^+ is subtracted following the dashed lines, and points are projected onto the predicted weathering trend. Grey zone 1 illustrates the range of CIA values possible for the studied samples; zone 2 illustrates the range of CIA values for most studied samples, varying from 63 to 83. Note that lines of “A1”, “A2” and “B” represent the predicted weathering trends for an initial fresh rock composition represented by the large black star and circle on the feldspar join. Line “C” is the retrograde alteration trend resulted from the kaolinite→illite→sericite transformation. Lines “D1” and “D2” represent metasomatic trends that are well removed from the predicted weathering trends; K-metasomatism would decrease the slopes of the lines. Data for basalt are from the average of 825–800 Ma basaltic rocks with LOI < 2 in the South China Block (Wang et al., 2009 and references therein). Data for granite are the average of ca. 825 Ma granites in North Guangxi (Li et al., 2003a). 50B50G mix represents a mixture of about 50% basalt and 50% granite.

Table 1 Sm-Nd isotopic compositions of Nanhua Rift Basin sedimentary and volcaniclastic rocks

Stratigraphic unit	Samples	Lithology	Tstrat[1] (Ga)	Nd (ppm)	Sm (ppm)	$^{147}Sm/^{144}Nd$	$^{143}Nd/^{144}Nd$	$\pm 2\sigma_m$ [2]	$e_{Nd(0)}$	$e_{Nd(t)}$	T_{DM}[3] (Ga)
Neoproterozoic											
Jiangkou Gr	08SC16	Tuf.slst	0.70	37.1	7.447	0.1213	0.512262	9	-7.3	-0.6	1.46
Jiangkou Gr	08SC15	Tuf.slst	0.70	31.11	5.579	0.1084	0.512089	8	-10.7	-2.8	1.53
Jiangkou Gr	08SC14	Tuf.slst	0.70	19.56	3.51	0.1085	0.512184	9	-8.8	-1	1.4
Jiangkou Gr	08SC58	Pel	0.70	28.44	5.32	0.1131	0.512267	10	-7.2	0.3	1.34
Jiangkou Gr	08SC59	Pel	0.70	44.18	7.204	0.0986	0.511879	11	-14.8	-6	1.68
Jiangkou Gr	08SC54	Pel	0.70	47.61	8.1308	0.1032	0.512136	9	-9.8	-1.4	1.4
Jiangkou Gr	08SC53	Pel	0.70	41.21	8.566	0.1257	0.512257	8	-7.4	-1.1	1.54
Fanzhao Fm	08SC07	Tul.slst	0.81	26.57	4.517	0.1028	0.512008	9	-12.3	-2.7	1.57
Fanzhao Fm	08SC04	Slst	0.81	53.11	10.63	0.121	0.512028	7	-11.9	-4.2	1.84
Fanzhao Fm	08SC03	Tul.slst	0.81	42	7.62	0.1097	0.511843	10	-15.5	-6.6	1.91
Fanzhao Fm	08SC02	Slst	0.81	53.01	9.338	0.1065	0.511885	7	-14.7	-5.5	1.79
Yanmenzhai Fm	08SC11	Tuf.slst	0.73	36.17	6.464	0.108	0.511941	7	-13.6	-5.3	1.74
Yanmenzhai Fm	08SC10	Tuf.slst	0.73	40.72	8.964	0.1331	0.512214	8	-8.3	-2.3	1.77
Yanmenzhai Fm	08SC09	Tuf.slst	0.73	25.57	4.982	0.1178	0.511998	9	-12.5	-5.1	1.83
Yanmenzhai Fm	08SC08	Tuf.slst	0.73	23.61	4.812	0.1232	0.512033	11	-11.8	-5	1.88
Qingshuijiang Fm	08SC32	Tuf.slst	0.78	14.39	3.719	0.1562	0.512382	13	-5	-1	2.03
Qingshuijiang Fm	08SC31	Tuf	0.78	47.74	8.283	0.1172	0.512291	7	-7.2	2.3	1.2
Qingshuijiang Fm	08SC30	Pel	0.78	44.26	9.066	0.1238	0.512123	6	-10	-2.9	1.74
Qingshuijiang Fm	08SC29	Pel	0.78	20.26	3.56	0.1062	0.511939	8	-13.6	-4.7	1.71
Qingshuijiang Fm	08SC25	Sst	0.78	32.15	5.897	0.1109	0.511935	8	-13.7	-5.3	1.8
Qingshuijiang Fm	08SC23	Sst	0.78	39.29	6.505	0.1001	0.512027	9	-11.9	-2.4	1.5
Qingshuijiang Fm	08SC21	Tuf.sst	0.78	49.47	8.95	0.1094	0.511842	7	-15.5	-6.9	1.9
Qingshuijiang Fm	08SC19	Tuf.slst	0.78	47.95	8.856	0.1116	0.511922	7	-14	-5.6	1.83
Pinglue Fm	08SC45	Sst	0.75	27.23	4.937	0.1096	0.512201	9	-8.5	-0.2	1.39
Pinglue Fm	08SC39	Pel.slst	0.75	63.11	14.18	0.1358	0.512081	5	-10.9	-5	2.08
Pinglue Fm	08SC36	Sst	0.75	42.73	8.692	0.123	0.512114	8	-10.2	-3.2	1.74
Pinglue Fm	08SC35	Sst	0.75	44.25	9.37	0.128	0.512128	10	-9.9	-3.4	1.81
Longli Fm	08SC50	Pel	0.72	95.32	16.86	0.1069	0.512083	7	-10.8	-2.6	1.52
Longli Fm	08SC47	Sst	0.72	95.58	17.9	0.1132	0.512209	7	-8.4	-0.7	1.43
Jialu Fm	08SC66	Sst	0.82	95.58	17.9	0.1132	0.512117	8	-10.2	-1.4	1.56
Jialu Fm	08SC63	Slst	0.82	95.58	17.9	0.1132	0.512086	13	-10.8	-2	1.61
Jialu Fm	08SC61	Sst	0.82	95.58	17.9	0.1132	0.511933	9	-13.8	-5	1.84

Jialu Fm	08SC60	Pel	0.82	95.58	17.9	0.1132	0.511995	7	-12.5	-3.8	1.75
Baizhu Fm	08SC70	Slst	0.82	50.51	9.483	0.1135	0.511929	8	-13.8	-5.1	1.85
Hetong Fm	08SC71-1	Pel	0.77	34.01	6.227	0.1107	0.511908	7	-14.2	-5.4	1.83
Gongdong Fm	08SC74	Slst	0.73	49.25	9.499	0.119	0.51209	8	-10.7	-3.2	1.7
Gongdong Fm	08SC75	Pel	0.73	27.8	4.087	0.0922	0.51225	8	-7.6	2.8	1.13

1. Stratigraphic ages are approximate and estimated based on comparison of regional stratigraphy and available chronological data as shown in Figure 2 (see text).
2. Isotope error measurements are 2 S.E.
3. Nd depleted mantle model ages were calculated using the following equation: $T_{DM} = (1/\lambda_{Sm}) \times \ln[1 + (0.51315 - {}^{143}Nd/{}^{144}Nd)/(0.2137 - {}^{147}Sm/{}^{144}Nd)]$; two-stage Nd model ages (T_{2DM}) were calculated for a few samples with $^{147}Sm/^{144}Nd$ ratios either > 0.13 or < 0.10 in order to minimise the bias of T_{DM} caused by significant Sm/Nd fractionation. The equation for the calculation of two-state Nd model ages is as in Li and McCulloch (1996).
4. Sst, sandstone; Slst, siltstone; Tuf, tuff; Tuf.slst, tuffaceous siltstone; Tuf.sst, tuffaceous sandstone; Pel., Pelite; Pel.slst, peliticsiltstone; Gr, Group; Fm, formation.

Table 2 Hf-Lu isotope data for the Nanhua Rift sedimentary and volcaniclastic rocks

Stratigraphic unit	Samples	Lithology	Tstrat (Ga)	Lu (ppm)	Hf (ppm)	$^{176}Lu/^{177}Hf$	$^{176}Hf/^{177}Hf$	$\pm 2\sigma_m$[1]	εHf(t)	T_{DM}[2] (Ga)	T_{2DM}[3] (Ga)
Jiangkou Gr	08SC59	Pel	0.7	0.48	14.51	0.005	0.282241	5	-5.6	1.58	1.95
Jiangkou Gr	08SC58	Pel	0.7	0.69	6.53	0.015	0.282575	7	1.5	1.52	1.52
Jiangkou Gr	08SC54	Pel	0.7	0.61	6.5	0.013	0.282559	5	1.7	1.45	1.51
Jiangkou Gr	08SC53	Pel	0.7	0.66	8.15	0.012	0.282582	6	3.3	1.32	1.4
Jiangkou Gr	08SC16	Tuf.slst	0.7	0.49	4.95	0.014	0.282455	8	-2.4	1.71	1.75
Jiangkou Gr	08SC15	Tuf.slst	0.7	0.48	5.72	0.012	0.282411	6	-3	1.67	1.79
Jiangkou Gr	08SC14	Tuf.slst	0.7	0.29	5.13	0.008	0.282525	13	3	1.27	1.43
Fanzhao Fm	08SC07	Tul.slst	0.81	0.45	5.73	0.011	0.282442	8	0.1	1.56	1.69
Fanzhao Fm	08SC04	Slst	0.81	0.64	8.04	0.011	0.282292	5	-5.3	1.86	2.02
Fanzhao Fm	08SC03	Tul.slst	0.81	0.61	6.83	0.013	0.282308	8	-5.5	1.93	2.04
Fanzhao Fm	08SC02	Slst	0.81	0.59	6.05	0.014	0.282409	6	-2.5	1.8	1.85
Yanmenzhai Fm	08SC11	Tuf.slst	0.73	0.49	5.68	0.012	0.282344	6	-5.4	1.82	1.94
Yanmenzhai Fm	08SC10	Tuf.slst	0.73	0.78	7.18	0.015	0.282606	7	2.2	1.48	1.47
Yanmenzhai Fm	08SC09	Tuf.slst	0.73	0.52	6.2	0.012	0.282422	6	-2.5	1.65	1.76
Yanmenzhai Fm	08SC08	Tuf.slst	0.73	0.42	4.58	0.013	0.282427	9	-2.8	1.7	1.78
Qingshuijiang Fm	08SC32	Tuf.slst	0.78	0.89	8.53	0.015	0.28265	6	5.1	1.34	1.35
Qingshuijiang Fm	08SC31	Tuf	0.78	1.09	9.49	0.016	0.282709	7	6.4	1.29	1.27
Qingshuijiang Fm	08SC30	Pel	0.78	0.86	9.29	0.013	0.282583	6	3.6	1.4	1.45
Qingshuijiang Fm	08SC29	Pel	0.78	0.67	8.15	0.012	0.282349	7	-3.9	1.77	1.91
Qingshuijiang Fm	08SC25	Sst	0.78	0.63	6.38	0.014	0.282377	6	-4.1	1.88	1.93
Qingshuijiang Fm	08SC21	Tuf.sst	0.78	0.9	9.06	0.014	0.282245	7	-9.1	2.17	2.22
Qingshuijiang Fm	08SC19	Tuf.slst	0.78	0.69	7.81	0.012	0.282328	5	-5.4	1.87	1.99
Pinglue Fm	08SC45	Sst	0.75	0.57	6.61	0.012	0.282574	9	3.4	1.37	1.44
Pinglue Fm	08SC39	Pel.slst	0.75	1.28	11.86	0.015	0.282475	5	-1.6	1.77	1.75
Pinglue Fm	08SC36	Sst	0.75	0.97	10.59	0.013	0.282503	8	0.6	1.55	1.62
Pinglue Fm	08SC35	Sst	0.75	0.79	6.85	0.016	0.282506	6	-1	1.77	1.71
Longli Fm	08SC50	Pel	0.72	0.86	9.23	0.013	0.282532	7	1	1.51	1.57
Longli Fm	08SC47	Sst	0.72	0.84	7.16	0.017	0.282627	12	2.8	1.51	1.46
Jialu Fm	08SC66	Sst	0.82	0.61	6.38	0.014	0.282568	7	3.5	1.45	1.49
Jialu Fm	08SC63	Slst	0.82	0.52	7.85	0.009	0.282328	8	-2.7	1.68	1.88
Jialu Fm	08SC61	Sst	0.82	0.46	5.91	0.011	0.282324	7	-3.7	1.78	1.94
Jialu Fm	08SC60	Pel	0.82	0.48	4.35	0.016	0.28245	8	-1.7	1.84	1.82
Baizhu Fm	08SC70	Slst	0.82	0.79	6.47	0.017	0.282409	6	-4.2	2.1	1.97

Hetong Fm	08SC71-1	Pel	0.77	0.61	7.94	0.011	0.282325	9	-3.6	1.77	1.93
Gongdong Fm	08SC75	Slst	0.73	0.23	4.14	0.008	0.282563	7	4.7	1.2	1.33
Gongdong Fm	08SC74	Pel	0.73	0.67	7.73	0.012	0.28245	6	-1.4	1.61	1.71

1. Isotope error measurements are 2 S.E.

2. Hf depleted mantle model ages (T^{DM}) were calculated using the following equation: T_{DM} = $(1/\lambda_{Lu}) \times \ln [1 + (^{176}Hf/^{177}Hf - 0.28325)/(^{176}Lu/^{177}Hf - 0.0384)]$.

3. Two-stage Hf model ages (T_{2DM}) were calculated using equation $T_{2DM} = T_{DM} - (T_{DM} - 0.72) \times [(-0.55 - (^{176}Lu/^{177}Hf/0.0332-1)/(-0.55-0.16)]$.

4. Gr, group; Fm, formation.

Appendix A Major and trace element data from the Neoproterozoic rift sequences in the Nanhua Rift Basin, South China Block.

Sample no.	08SC60	08SC63	08SC66	08SC61	08SC64	08SC02	08SC03	08SC04	08SC05	08SC06	08SC07
Stratigraphic	Jialu Fm			Wuye Fm		Fanzhao Fm					
Lithology	Pel	Slst	Sst	Sst	Pel	Slst	Tul.slst	Slst	Tul.slst	Slst	Tul.slst
SiO_2	62.5	67.5	73.8	70.2	67.2	65	66.8	63.1	75.3	77.3	75.5
TiO_2	0.82	0.72	0.83	0.79	0.83	0.91	0.93	0.84	0.42	0.47	0.79
Al_2O_3	15.6	16.7	13.9	17	18.7	22.1	20.3	20.7	17.8	15.3	19.2
CaO	0.06	0.57	0.15	0.13	0.33	0.05	0.05	0.13	0.05	0.06	0.05
Fe_2O_3*	13.9	5.9	5.89	4.29	5.83	7.32	7.41	8.08	1.11	4.03	0.47
K_2O	3.31	2.28	2.65	3.9	3.92	3.38	3.72	3.75	4.4	2.52	3.52
MgO	3.58	2.82	1.6	2.05	1.91	1.05	0.5	1.6	0.68	0.3	0.41
MnO	0.06	0.2	0.07	0.04	0.08	0.05	0.01	0.09	0.03	0.01	0
Na_2O	0.17	3.19	1.04	1.54	1.17	0.11	0.08	1.65	0.12	0.05	0.08
P_2O_5	0.05	0.11	0.06	0.07	0.05	0.06	0.11	0.07	0.03	0.03	0.02
Total	99.4	99.6	99.6	99.6	99.6	99.9	99.8	99.7	99.6	99.5	99.7
CIA	79.7	74.1	73.4	65.6	70.9	84.9	82.7	74.8	77.9	84	82.6
LOI	3.66	2.4	2.9	2.72	3.14	6.03	5.43	4.35	3.35	4.15	4.38
Sc	14.2	15.6	23.7	11.2	13.2	17.1	12.6	17.7	8.38	8.09	12.9
Ti	4081	4100	4006	3705	3837	4661	4743	4366	2262	2578	4068
V	134	116	126	97.8	128	54.4	52.3	102	39.8	58.7	104
Cr	56.4	59.1	102	41.4	118	57.9	39.6	34.1	23.7	33.7	60.9
Mn	425	483	534	1498	247	313	19.2	685	220	35.8	0.762
Co	16.7	19.4	18.5	47.5	6.85	12.7	2.729	7.62	1.08	2.74	10.7
Ni	28.4	56.2	34.8	35	15.7	43.6	20.5	48.1	9.7	17.4	15.6
Cu	109	21.5	3.4	5.4	5.89	30.2	23.3	24.6	6.01	13.7	12.2
Zn	434	85.5	86.7	154	62.1	126	42.9	124	43.4	32.3	24.2
Ga	21.7	16.1	23.4	20.6	22.2	27.1	26.9	29	22.7	17.8	22
Ge	4.97	2.33	3.12	2.95	2.08	2.72	2.47	2.8	2.06	2.63	2.56
Rb	179	108	155	93.8	142	112	123	122	148	81.2	106
Sr	25.3	26.4	70.2	76.3	68.5	19.4	19.9	54.1	19.3	12.7	15.6
Y	28.1	24.3	28.2	21.5	22	39.7	37.3	41.2	38.4	25.6	26.3
Zr	147	261	200	178	190	233	254	301	240	167	208
Nb	10.6	11.8	12.8	14.7	13.6	13.4	14.8	15.9	13.7	12.6	15
Ba	946	404	1043	618	1012	794	842	800	1178	667	849
La	54	15.4	36.1	38.3	41.1	59.6	48.2	55.2	54.9	36.2	37.8
Ce	106	33.4	77.7	81.7	80.8	118	94.9	112	110	72.1	69.6
Pr	12.6	4.37	9.4	9.74	9.88	14	11.3	13.7	13.2	8.65	7.7
Nd	44.8	16.7	34.7	35.7	36.3	53	42	53.1	48.8	31.1	26.6
Sm	8.34	3.48	6.36	6.97	6.64	9.34	7.62	10.6	8.76	5.83	4.52

Eu	1.6	0.756	1.31	1.66	1.1	2.01	1.68	2.21	1.73	1.17	0.97
Gd	7.28	3.59	5.65	5.68	5.3	8	7	8.9	7.51	4.63	4.51
Tb	1.04	0.678	0.946	0.799	0.785	1.23	1.09	1.27	1.16	0.75	0.762
Dy	5.86	4.56	5.71	4.15	4.41	7.07	6.68	7.31	6.82	4.51	4.77
Ho	1.16	0.998	1.19	0.86	0.938	1.46	1.38	1.48	1.41	0.902	1.01
Er	3.13	2.98	3.43	2.59	2.73	4	3.88	4.05	3.98	2.56	2.84
Tm	0.468	0.463	0.548	0.419	0.434	0.59	0.582	0.627	0.6	0.41	0.431
Yb	3.08	3.09	3.83	2.89	3.13	3.84	3.92	4.04	4.13	2.77	2.86
Lu	0.476	0.522	0.609	0.456	0.518	0.588	0.614	0.637	0.655	0.435	0.449
Hf	4.35	7.85	6.38	5.91	6.07	6.05	6.83	8.04	6.89	4.87	5.73
Ta	0.866	1.08	1.17	1.16	1.13	0.913	1.01	1.08	1.07	0.928	1.11
Pb	12.9	7.2	19.6	16.1	20.8	12.2	8.7	20.6	15.4	23.8	27
Th	14.1	12.7	15	12.2	11.7	10.2	10.8	11.7	12.3	10.9	12.8
U	2.84	2.74	2.75	1.88	2.1	1.78	1.93	2.67	2.8	2.12	3.31
Th/Sc	0.993	0.817	0.632	1.09	0.887	0.6	0.855	0.66	1.47	1.35	0.994
La_N/Yb_N	12.6	3.57	6.76	9.5	9.44	11.1	8.82	9.78	9.53	9.39	9.48
Sm_N/Yb_N	3	1.25	1.85	2.68	2.36	2.7	2.16	2.92	2.36	2.34	1.75
Eu/Eu*	0.626	0.654	0.668	0.807	0.567	0.712	0.705	0.696	0.651	0.686	0.657
La_N/Sm_N	4.19	2.86	3.67	3.55	4	4.12	4.08	3.35	4.04	4.01	5.41
Gd_N/Yb_N	1.95	0.96	1.22	1.62	1.4	1.72	1.48	1.82	1.51	1.38	1.31
Sample no.	08SC17	08SC18	08SC19	08SC21	08SC23	08SC25	08SC29	08SC30	08SC31	08SC32	08SC33
Stratigraphic	Qingshuijiang Fm										
Lithology	Tuf	Tuf	Tuf.slst	Tuf.sst	Sst	Sst	Pel	Pel	Tuf	Tuf.slst	Tuf
SiO_2	80.5	80.2	67.9	67.1	70.6	73.1	68.5	61.9	73.4	69.8	64.1
TiO_2	0.34	0.31	0.96	0.62	0.7	0.52	0.77	0.91	0.47	0.66	0.78
Al_2O_3	10.9	11.7	18.1	19.6	16.9	15.2	17.1	20.4	16.5	17.9	21
CaO	0.1	0.1	0.13	0.1	0.18	0.38	0.24	0.56	0.26	0.31	0.25
Fe_2O_3*	2.51	2.41	5.25	4.26	4.27	3.51	5.29	6.37	2.13	3.31	4.81
K_2O	0.34	1.79	4.59	4.95	3.2	2.87	3.8	5.98	5.07	4.6	4.82
MgO	0.44	0.63	1.48	1.33	1.06	0.89	1.36	1.76	0.99	1.14	1.47
MnO	0.05	0.02	0.04	0.03	0.02	0.04	0.09	0.11	0.03	0.05	0.08
Na_2O	4.82	2.81	1.52	1.91	2.97	3.41	2.78	1.9	1.08	2.16	2.63
P_2O_5	0.04	0.06	0.06	0.05	0.09	0.09	0.1	0.13	0.06	0.09	0.08
Total	99.5	99.5	99.5	99.7	99.6	99.6	99.6	99.6	99.6	99.6	99.8
CIA	56.2	63.4	70.1	69.3	66.1	61.8	65.2	65.8	68.2	66.3	67.8
LOI	0.907	1.54	3.04	3.07	2.25	2	2.74	3.02	2.43	2.48	3
Sc	5.82	5.22	17.9	13.4	14.4	7.8	14.3	19.3	19.3	14.8	17.9
Ti	1735	1701	5183	3525	3902	2834	4040	4840	2471	3599	4351
V	33.5	31.5	121	83.6	92.4	66.7	84.2	105	139	99.3	85.3
Cr	20.7	19	59.6	14.8	60.1	47.8	67.6	58.9	89.2	97.9	47.6

Mn	308	156	248	210	177	252	707	856	223	437	618
Co	4.39	2.85	7.31	9.09	5.73	10.8	7.12	10.9	18	17.8	5
Ni	10.1	5.55	22.8	12.1	16.4	17.9	21.4	22	82	54.8	18.3
Cu	13	17.9	5.66	8.42	12.9	15.3	12.2	16	2.65	11.8	8.13
Zn	41.4	37.3	74.7	61.3	57.8	80	91.9	117	53.4	55.8	91.9
Ga	7.38	12.1	27.5	35.5	23.7	21.2	27.3	30.2	28.4	25.6	36.1
Ge	1.35	1.82	2.88	2.62	2.26	2.12	1.97	3.11	2.02	1.91	1.86
Rb	9.19	53.3	136	149	99.7	87	106	166	141	125	134
Sr	104	75.6	60.3	64.3	97.1	91.9	132	98.5	43.3	102	118
Y	18	18.5	39.2	50.5	34.2	30.6	27.7	45.4	50.9	37.7	42.1
Zr	139	136	277	267	251	200	285	324	286	294	372
Nb	7.92	8.67	13.7	20.4	13	14.4	13.2	13	13.6	9.87	15.2
Ba	146	548	1394	1477	915	885	1106	1473	1168	1343	1579
La	25.1	35.2	51.1	49.7	42.3	38.7	20.9	40.1	36.1	8.15	12.9
Ce	48.9	68.1	104	106	85.5	77.8	44.1	87.7	83.8	21.2	28.2
Pr	5.73	7.94	12.8	13.1	10.4	8.93	5.62	11.2	11.7	3.34	3.72
Nd	21	27.5	48	49.5	39.3	32.2	20.3	44.3	47.7	14.4	15
Sm	3.66	4.77	8.86	9.95	7.3	5.9	3.56	9.07	8.28	3.72	3.53
Eu	0.754	0.977	1.84	1.56	1.56	1.2	0.927	2.14	1.54	0.928	0.829
Gd	3.31	3.87	7.86	9.2	6.55	5.28	3.31	8.38	7.43	4.18	4.24
Tb	0.524	0.6	1.26	1.51	1.05	0.851	0.571	1.39	1.41	0.89	0.944
Dy	3.09	3.38	7.56	9.18	6.38	5.18	4.14	8.35	9.24	6.32	7.28
Ho	0.645	0.697	1.58	1.96	1.34	1.12	1.08	1.77	2.03	1.54	1.79
Er	1.89	1.98	4.39	5.58	3.83	3.34	3.57	5.1	6.02	4.81	5.46
Tm	0.297	0.302	0.66	0.85	0.58	0.537	0.583	0.775	0.967	0.769	0.867
Yb	2.06	2.12	4.37	5.58	3.95	3.71	4.04	5.2	6.74	5.36	5.9
Lu	0.326	0.343	0.687	0.903	0.619	0.628	0.67	0.864	1.09	0.891	0.969
Hf	3.81	3.82	7.8	9.06	7.24	6.38	8.15	9.29	9.49	8.53	10.9
Ta	0.551	0.59	1.02	1.62	0.895	1.05	0.901	0.84	1.01	0.726	1.09
Pb	13.3	18.9	3.18	22.4	10.8	21.2	17.8	21.8	4.46	5.6	9.6
Th	4.83	4.8	11.1	23.1	9.03	9.65	9.58	9.37	10.8	6.8	11.1
U	1.08	1.1	2.06	4.17	1.91	2.01	1.86	1.4	2.02	1.17	2.24
Th/Sc	0.829	0.918	0.619	1.73	0.627	1.24	0.668	0.485	0.561	0.461	0.619
La_N/Yb_N	8.73	11.9	8.38	6.38	7.68	7.48	3.71	5.53	3.84	1.09	1.57
Sm_N/Yb_N	1.97	2.49	2.25	1.98	2.05	1.77	0.98	1.94	1.37	0.771	0.664
Eu/Eu*	0.662	0.695	0.673	0.499	0.691	0.657	0.826	0.752	0.6	0.72	0.655
La_N/Sm_N	4.43	4.77	3.72	3.22	3.74	4.24	3.78	2.85	2.81	1.42	2.36
Gd_N/Yb_N	1.33	1.51	1.49	1.36	1.37	1.18	0.678	1.33	0.911	0.646	0.595
Sample no.	08SC35	08SC36	08SC39	08SC40	08SC41	08SC42	08SC43	08SC45	08SC47	08SC48	08SC49
Stratigraphic	Pinglue Fm								Longli Fm		

Lithology	Sst	Sst	Pel.slst	Pel	Tuf	Tuf.slst	Tuf.sst	Sst	Sst.	Pel.	Pel.
SiO_2	70.2	66.5	59.9	68.5	69.7	74.2	67.6	69.8	66.9	68.8	70.8
TiO_2	0.66	0.95	0.68	0.73	0.77	0.64	0.81	0.78	0.88	0.77	0.65
Al_2O_3	17.1	20.4	24.3	17.7	17.8	14.7	17.7	16.8	20	16.9	16.6
CaO	0.42	0.17	0.29	0.6	0.61	0.65	0.76	0.22	0.09	0.34	0.2
Fe_2O_3*	4.35	4.11	5.3	4.86	4.07	3.06	5.63	5.19	5.97	5.49	5.09
K_2O	3.64	4.36	6.17	2.47	3.88	2.07	2.98	2.31	4.19	3.51	3.14
MgO	1.07	1.07	1.62	0.75	0.98	0.82	1.86	1.68	1.75	1.92	1.47
MnO	0.06	0.05	0.06	0.07	0.06	0.06	0.07	0.06	0.04	0.06	0.11
Na_2O	2.51	2.33	1.48	4.25	2.1	3.73	2.48	2.99	0.1	2.05	1.84
P_2O_5	0.06	0.03	0.17	0.04	0.04	0.04	0.12	0.11	0.06	0.13	0.1
Total	99.6	99.8	99.9	99.6	99.7	99.6	99.7	99.7	99.8	99.6	99.6
CIA	65.9	69.8	71.6	62.2	66.9	60.6	67	68.3	80.5	68.4	71
LOI	2.62	3.76	4.3	2.43	2.47	1.51	3	2.53	5.1	2.68	2.63
Sc	14.7	19.7	20.1	11.6	12.3	10.3	14.3	16.8	18	13.7	13
Ti	3616	5165	4021	3977	4275	3331	4185	3971	4506	3938	3265
V	83.5	96.3	80	56	90	67.3	123	120	147	111	99.7
Cr	53.8	66.9	28.6	29.7	53.4	44.8	55.2	74.3	93.4	67.9	43.1
Mn	500	313	539	539	440	419	548	408	265	485	870
Co	4.21	3.87	4.85	3.7	15.4	4.26	8.77	12.9	11.6	24.8	9.52
Ni	19.6	14.6	19.8	5.87	21.5	8.26	21.1	57.4	48.1	28.5	22
Cu	11.2	13.4	13.7	12.9	10.9	10.8	20.2	21.3	44.1	33	21.4
Zn	92	113	66.9	77.8	72.8	43.5	87.5	67.2	172	94.4	91.7
Ga	25.6	34.2	35.5	26.7	23	16.8	22.7	19.6	25.5	21.6	22.4
Ge	2.3	2.09	3.4	2.23	2.5	2.14	2.29	2.24	2.27	2.06	2.28
Rb	101	110	190	63.1	118	64.6	103	81.1	142	116	109
Sr	97	82.6	118	198	125	219	160	133	24.3	127	96
Y	46	43.3	85.5	52.8	38.2	38.8	33.5	28.2	55.3	41.6	31.8
Zr	236	361	384	383	267	272	230	228	237	209	196
Nb	10.8	15.7	17.8	12.2	12.1	10.1	11.4	11.1	13.2	12.4	9.86
Ba	1047	1224	1553	742	1323	773	837	584	877	864	555
La	41.2	36.5	57.5	12.4	40.4	58	26.1	29.4	88.6	71.6	37.2
Ce	87.8	80.2	123	33.8	83.1	116	59.2	59	190	150	86.1
Pr	11.3	10.6	15.8	5.52	10.7	13.9	8.09	7.41	24.4	18.3	12
Nd	44.2	42.7	63.1	26.5	41.1	52.7	31.5	27.2	95.6	68.7	47.8
Sm	9.37	8.69	14.2	7.12	7.94	9.32	6.66	4.94	17.9	12.1	8.89
Eu	2.56	2.61	3.15	1.98	2.05	2.32	1.57	1.29	3.78	2.64	2.3
Gd	9.11	7.95	14.8	8.03	7.38	8.23	6.29	4.68	14.8	10.2	8.08
Tb	1.57	1.3	2.72	1.46	1.2	1.33	1.05	0.793	2.15	1.51	1.22
Dy	9.34	7.91	16.9	9.36	7.12	7.92	6.4	4.81	11.5	8.27	6.66
Ho	1.87	1.69	3.4	2.1	1.48	1.58	1.36	1.06	2.24	1.63	1.3

Er	5.1	5.03	8.89	5.96	4.08	4.3	3.88	3.21	5.85	4.4	3.54
Tm	0.754	0.811	1.33	0.896	0.613	0.645	0.589	0.513	0.843	0.657	0.531
Yb	4.96	5.68	8.36	5.9	4.17	4.17	3.93	3.52	5.37	4.37	3.56
Lu	0.788	0.968	1.28	0.928	0.654	0.656	0.616	0.572	0.842	0.702	0.566
Hf	6.85	10.6	11.9	10.3	7.73	7.25	6.53	6.6	7.16	6.4	5.8
Ta	0.8	1.14	1.27	0.903	0.893	0.668	0.89	0.922	1.12	1.03	0.797
Pb	8.87	16.4	2.48	10.9	6.74	13.8	7.5	7.31	8.9	64.6	13.2
Th	8.8	11.1	12.7	10	9.32	7.84	11	10.7	15.4	11.7	10.5
U	1.7	2.26	2.56	1.94	1.89	1.78	2.36	2.44	3.34	2.53	1.85
Th/Sc	0.598	0.566	0.631	0.862	0.756	0.764	0.767	0.638	0.856	0.849	0.803
La_N/Yb_N	5.96	4.61	4.93	1.51	6.95	9.98	4.76	6.01	11.8	11.8	7.5
Sm_N/Yb_N	2.1	1.7	1.88	1.34	2.12	2.48	1.88	1.56	3.7	3.07	2.77
Eu/Eu*	0.875	0.877	0.663	0.801	0.817	0.81	0.743	0.818	0.711	0.726	0.829
La_N/Sm_N	2.84	2.71	2.62	1.13	3.28	4.02	2.53	3.85	3.2	3.83	2.7
Gd_N/Yb_N	1.52	1.16	1.47	1.13	1.47	1.63	1.32	1.1	2.28	1.94	1.88

Sample no.	08SC50	08SC52	08SC53	08SC54	08SC55	08SC56	08SC14	08SC15	08SC16
Stratigraphic	Longli Fm		Jiakou Gr (Guizhou)				Jiakou Gr (Cahng'an Fm, Hunan)		
Lithology	Pel.	Sst	Pel.	Pel.	Pel	Pel	Tuf.slst	Tuf.slst	Tuf.slst
SiO_2	65.6	87.7	65.9	64.9	73.4	71.9	72.3	71.8	75
TiO_2	0.92	0.69	0.9	0.82	0.66	0.73	0.53	0.57	0.46
Al_2O_3	22.2	6.75	22.1	20.3	16	18.3	13.3	14.7	12.7
CaO	0.13	0.05	0.05	0.06	0.12	0.07	0.28	0.78	1.42
Fe_2O_3*	3.18	3.62	5.86	7.65	4.6	3.7	5.18	4.51	4.56
K_2O	5.43	0.61	3.65	4.64	2.78	2.7	0.06	2.68	2.43
MgO	1.56	0.55	1.27	1.23	1.27	1.5	1.53	0.91	1.43
MnO	0.05	0.01	0.05	0.03	0.05	0.1	0.06	0.02	0.13
Na_2O	0.94	-0.02	0.13	0.27	1.05	1	6.66	4.02	1.54
P_2O_5	0.04	0.02	0.05	0.06	0.05	0.04	0.09	0.09	0.38
Total	99.8	99.3	99.8	99.7	99.6	99.7	99.5	99.6	99.5
CIA	74.3	90.2			76.4	79.6	53.6	57.3	62.1
LOI	4.07	2.34	5.4	4.19	3.64	4.02	1.06	1.88	2.2
Sc	28.7	5.12	18.5	15.2	9.19	10.8	15.6	15.5	18.7
Ti	4902	3455	4929	4196	3337	3763	2782	3254	2550
V	93.6	36.8	127	119	85	109	98.1	78.3	132
Cr	69.8	35	69.5	82.4	53.2	45.7	81.9	37.1	49.2
Mn	324	77.2	369	204	314	746	499	168	1104
Co	4.41	3.36	24.3	18	8.43	13	15	20	19.2
Ni	14.2	12.6	56.2	65.9	18.5	20.9	63.1	42.8	67.8
Cu	18.2	19.9	27.1	24.2	14.5	25.6	4.53	5.98	34.1
Zn	61.1	34.5	136	214	76.4	69.4	63.3	53.3	96.2

Ga	30.1	7.32	26	25.6	19.9	21.4	12.7	17.9	16.8
Ge	2.57	2.49	3.52	3.26	2.36	2.59	1.23	1.61	2.47
Rb	169	18.7	133	174	95.9	97.5	0.94	88.5	74.6
Sr	85.8	9.79	45.6	80	60.6	79	106	132	124
Y	53.6	18.7	35.1	34.2	40	24	16.2	27.2	29.8
Zr	328	288	270	216	221	246	196	218	189
Nb	15	10.5	13.9	13.2	10.8	10.6	7.93	9.69	8.43
Ba	1172	178	874	1000	769	887	28.5	609	635
La	103	29.4	41.6	45.6	46.1	69.4	24	35.4	29.4
Ce	211	58.1	86.3	96.9	94.6	124	45.8	70.1	66
Pr	26.2	6.9	10.8	12.4	11.7	13.4	5.25	8.36	9.02
Nd	95.3	24.5	41.2	47.6	44.9	43.6	19.6	31.1	37.1
Sm	16.9	4.12	8.57	8.61	8.83	7.37	3.51	5.58	7.45
Eu	3.68	0.928	2	1.83	2.05	1.78	0.87	1.35	1.68
Gd	12.8	3.8	8.25	7.41	8.24	5.4	3.21	4.97	6.52
Tb	1.92	0.589	1.37	1.11	1.35	0.853	0.497	0.794	1.01
Dy	10.5	3.48	7.81	6.61	7.85	4.98	2.99	4.83	5.63
Ho	2.11	0.727	1.54	1.37	1.64	1.03	0.634	1.01	1.15
Er	5.55	2.03	4.19	3.83	4.43	3.03	1.77	2.86	3.03
Tm	0.819	0.322	0.627	0.579	0.668	0.479	0.266	0.446	0.446
Yb	5.35	2.16	4.05	3.88	4.39	3.28	1.81	2.94	2.92
Lu	0.864	0.346	0.662	0.609	0.712	0.546	0.293	0.48	0.485
Hf	9.23	7.75	8.14	6.5	6.5	6.77	5.13	5.72	4.95
Ta	1.11	0.829	1.08	1.08	0.859	0.784	0.516	0.642	0.612
Pb	10.1	2.65	86.3	11.8	4.73	5.82	3.77	4.72	22.8
Th	12.4	9.38	12.8	14.6	10.6	9.21	5.29	7.57	7.04
U	2.63	1.47	2.16	1.7	2.22	1.49	1.11	1.07	1.44
Th/Sc	0.744	1.83	0.691	0.957	1.15	0.855	0.339	0.487	0.376
La_N/Yb_N	13.8	9.79	7.38	8.44	7.54	15.2	9.51	8.65	7.23
Sm_N/Yb_N	3.5	2.12	2.35	2.47	2.23	2.5	2.15	2.11	2.83
Eu/Eu*	0.766	0.717	0.728	0.699	0.733	0.864	0.792	0.785	0.737
La_N/Sm_N	3.93	4.62	3.14	3.42	3.37	6.08	4.42	4.1	2.55
Gd_N/Yb_N	1.99	1.46	1.69	1.58	1.55	1.36	1.46	1.4	1.85

Sample no.	08SC08	08SC09	08SC10	08SC11	08SC68-1	08SC70	08SC71-1	08SC74	08SC75
Stratigraphic	Yanmenzhai Fm,Banxi Gr				Siabo Gr	Baizhu Fm	Hetong Fm	Gongdong Fm	Gongdong Fm
Lithology	Tuf.slst	Tuf.slst	Tuf.slst	Tuf.slst	Slst	Slst	Pel	Slst	Pel
SiO_2	77.2	71.7	69.6	74	75.3	67.2	70.8	82.1	70.7
TiO_2	0.56	0.74	0.93	0.54	0.64	0.63	0.64	0.41	0.75
Al_2O_3	12.3	15.2	15.8	14.6	12.4	16.4	17.2	9.77	16.1

CaO	0.26	0.32	1.07	0.35	0.09	0.13	0.16	0.14	0.32
Fe_2O_3*	4.15	5.18	5.18	3.42	6.13	7.54	3.08	2.81	4.15
K_2O	2.07	2.64	2.72	2.08	2.71	2.7	3.13	0.71	1.74
MgO	0.94	1.1	1.21	0.99	1.79	3.57	1.26	1.08	1.99
MnO	0.06	0.05	0.09	0.04	0.03	0.14	0.03	0.06	0.11
Na_2O	2.35	2.94	3.02	3.88	0.79	1.64	3.62	2.89	4.06
P_2O_5	0.16	0.19	0.41	0.09	0.06	0.1	0.04	0.04	0.11
Total	99.4	99.6	99.6	99.6	99.4	99.6	99.6	99.4	99.6
CIA	65.2	64.7	61.5	61.1	73.8	73.7	64.1	62.9	63.8
LOI	1.83	2.78	2.59	1.78	2.46	3.37	2.67	1.66	2.14
Sc	11.5	11.3	16.6	10.5	9.15	10.8	8.24	21.1	28.7
Ti	2956	4014	4907	2891	3003	3003	3067	1906	3612
V	69.9	102	100	60	120	50.1	78.9	54.2	169
Cr	55.8	70.3	72.6	48.9	87.8	99.2	54.5	71.4	90.4
Mn	442	438	694	256	189	968	143	372	787
Co	3.32	9.17	12.7	7.76	21.5	9.82	10.6	11.8	28.8
Ni	11	21.2	34.7	19.3	48.7	37.5	34.6	15	129
Cu	7.38	12.2	14.2	18.3	46	26.1	24.4	30.7	27.1
Zn	67.9	56.6	101	63.4	82.3	88.6	37.3	56.1	75.4
Ga	16.5	20.2	21.4	18.8	14.2	23.6	20.4	8.99	17.3
Ge	1.95	2.32	2.2	1.92	2.8	2.72	1.75	1.57	1.99
Rb	55.3	74.8	75.7	60.1	126	103	101	25	60.6
Sr	73.7	96.8	132	129	26.2	62.9	115	76.4	180
Y	23.3	28.7	46.7	26.7	19	42.1	33.6	12.4	35
Zr	180	219	253	211	152	237	258	147	261
Nb	8.21	11.1	12.3	9.37	8.71	13.4	14.6	6.46	10.8
Ba	556	689	680	610	582	1203	1002	148	506
La	22.4	26.8	34.7	38.5	13.9	55.9	35.3	32	43
Ce	48.1	54.5	75.8	78.4	29.4	112	73	65.8	93.2
Pr	6.05	6.7	9.91	9.51	3.73	13.6	8.94	7.72	12.2
Nd	23.6	25.6	40.7	36.2	14.4	50.5	34	27.8	49.2
Sm	4.81	4.98	8.96	6.46	2.9	9.48	6.23	4.09	9.5
Eu	1.367	1.21	1.97	1.38	0.761	1.79	1.18	1.01	2.09
Gd	4.49	4.58	8.94	5.62	3.24	8.44	5.84	3.26	8.47
Tb	0.745	0.805	1.4	0.833	0.596	1.31	1.03	0.475	1.3
Dy	4.42	5.07	8.3	4.9	3.76	7.79	6.51	2.59	7.33
Ho	0.897	1.14	1.71	1.03	0.805	1.67	1.4	0.519	1.46
Er	2.59	3.25	4.87	2.85	2.32	4.87	3.97	1.39	4.24
Tm	0.41	0.501	0.749	0.45	0.359	0.762	0.58	0.21	0.634
Yb	2.63	3.37	5	2.97	2.45	5.04	3.92	1.43	4.22
Lu	0.415	0.523	0.781	0.49	0.394	0.792	0.607	0.233	0.668

Hf	4.58	6.2	7.18	5.68	4.66	6.47	7.94	4.14	7.73
Ta	0.557	0.765	0.831	0.626	0.787	0.99	1.13	0.518	0.88
Pb	0.893	24.6	5.19	10.7	15.7	13	25.2	6.44	4.68
Th	6.12	8.14	7.6	6.61	8.59	12.3	11.2	6.75	9.63
U	0.98	1.44	1.52	1.28	1.76	3.5	2.52	1.36	2.95
Th/Sc	0.532	0.723	0.457	0.627	0.939	1.14	1.36	0.32	0.336
La_N/Yb_N	6.1	5.71	4.99	9.29	4.08	7.95	6.47	16	7.31
Sm_N/Yb_N	2.03	1.64	1.99	2.42	1.32	2.09	1.77	3.17	2.5
Eu/Eu*	0.88	0.775	0.673	0.698	0.759	0.613	0.597	0.845	0.712
La_N/Sm_N	3	3.47	2.5	3.85	3.1	3.81	3.66	5.06	2.93
Gd_N/Yb_N	1.41	1.13	1.48	1.56	1.09	1.38	1.23	1.88	1.66

Sst, sandstone; Slst, siltstone; Tuf, tuff; Tuf.slst, tuffaceous siltstone; Tuf.sst, tuffaceous sandstone; Pel., Pelite; Pel.slst, peliticsiltstone; LOI, loss of ignition. Gr, group; Fm, formation.

Appendix C

Correlation coefficient parameters for the sedimentary rocks from Nanhua Rift, South China

	SiO_2	TiO_2	Al_2O_3	CaO	Fe_2O_3	K2O	MgO	MnO	Na_2O	CIA	Sc	Ti	V	Cr	Co
SiO_2	1.00														
TiO_2	-0.76	1.00													
Al_2O_3	-0.82	0.57	1.00												
CaO	-0.21	0.10	-0.16	1.00											
Fe_2O_3	-0.59	0.47	0.15	0.06	1.00										
K_2O	-0.68	0.45	0.81	-0.08	0.09	1.00									
MgO	-0.50	0.31	0.02	0.40	0.66	0.06	1.00								
MnO	-0.31	0.15	-0.02	0.44	0.33	-0.09	0.69	1.00							
Na_2O	0.25	-0.33	-0.27	0.04	-0.25	-0.45	-0.11	0.15	1.00						
CIA	-0.05	0.26	0.24	-0.54	0.18	0.24	-0.11	-0.32	-0.79	1.00					
Sc	-0.52	0.45	0.56	0.26	0.27	0.31	0.50	0.37	-0.06	-0.16	1.00				
V	-0.43	0.49	0.46	0.20	0.31	0.29	0.66	0.29	-0.17	-0.07	0.64	0.43	1.00		
Cr	-0.17	0.33	0.38	-0.05	0.16	0.11	0.46	0.10	-0.08	0.01	0.43	0.22	0.59	1.00	
Co	-0.16	0.24	0.34	0.17	0.26	-0.09	0.47	0.53	0.04	-0.19	0.34	0.07	0.55	0.33	1.00
Ni	-0.20	0.23	0.10	0.26	0.24	-0.06	0.39	0.34	0.00	-0.18	0.60	0.07	0.65	0.48	0.63
Rb	-0.71	0.48	0.76	-0.13	0.33	0.91	0.24	-0.07	-0.59	0.39	0.28	0.51	0.39	0.19	0.06
Sr	-0.10	0.00	-0.02	0.46	-0.15	-0.13	0.07	0.34	0.68	-0.77	0.19	0.03	0.09	-0.05	0.05
Y	-0.63	0.34	0.69	0.09	0.07	0.71	0.06	0.03	-0.19	0.07	0.33	0.45	0.12	-0.07	-0.19
Zr	-0.46	0.47	0.59	-0.01	-0.07	0.57	-0.11	0.00	-0.02	0.07	0.30	0.56	0.03	-0.07	-0.25
Nb	-0.65	0.46	0.69	0.05	0.13	0.68	0.19	0.02	-0.36	0.26	0.22	0.53	0.11	-0.10	-0.04
Ba	-0.62	0.36	0.75	-0.08	0.03	0.91	0.06	-0.06	-0.30	0.16	0.18	0.44	0.14	0.07	-0.17
La	-0.36	0.26	0.42	-0.07	0.11	0.34	0.18	-0.03	-0.37	0.35	0.11	0.27	0.10	0.01	-0.06
Sm	-0.55	0.37	0.56	0.04	0.17	0.51	0.21	0.10	-0.31	0.20	0.31	0.41	0.24	0.04	-0.03
Eu	-0.55	0.43	0.57	0.10	0.15	0.47	0.17	0.14	-0.23	0.13	0.31	0.48	0.22	0.01	-0.02
Gd	-0.60	0.39	0.60	0.09	0.18	0.56	0.20	0.11	-0.28	0.15	0.34	0.45	0.24	0.00	-0.05
Yb	-0.62	0.36	0.70	0.07	0.02	0.76	0.08	0.06	-0.14	0.02	0.36	0.45	0.18	0.06	-0.14
Lu	-0.61	0.36	0.70	0.06	0.01	0.77	0.08	0.07	-0.13	0.01	0.37	0.45	0.19	0.07	-0.13
Hf	-0.50	0.45	0.64	-0.02	-0.07	0.66	-0.05	0.01	-0.06	0.06	0.34	0.53	0.13	-0.02	-0.15
Th	-0.51	0.40	0.52	-0.17	0.32	0.54	0.31	-0.02	-0.52	0.48	0.22	0.39	0.30	0.05	0.12
U	-0.40	0.30	0.46	-0.15	0.15	0.40	0.29	-0.02	-0.37	0.42	0.20	0.27	0.28	0.10	0.04

	Ni	Rb	Sr	Y	Zr	Nb	Ba	La	Sm	Eu	Gd	Yb	Lu	Hf	Th	U
SiO_2																
TiO_2																
Al_2O_3																
CaO																
Fe_2O_3																
K_2O																
MgO																
MnO																
Na_2O																
CIA																
Sc																
V																
Cr																
Co																
Ni	1.00															
Rb	0.01	1.00														
Sr	0.10	-0.27	1.00													
Y	0.01	0.57	0.18	1.00												
Zr	-0.04	0.35	0.25	0.72	1.00											
Nb	-0.05	0.61	-0.17	0.61	0.54	1.00										
Ba	-0.18	0.80	0.00	0.67	0.59	0.64	1.00									
La	-0.07	0.41	-0.17	0.43	0.08	0.35	0.26	1.00								
Sm	0.06	0.51	0.01	0.75	0.34	0.45	0.40	0.86	1.00							
Eu	0.03	0.44	0.14	0.75	0.41	0.36	0.36	0.79	0.95	1.00						
Gd	0.06	0.53	0.09	0.86	0.44	0.49	0.46	0.74	0.97	0.95	1.00					
Yb	0.04	0.60	0.21	0.94	0.79	0.62	0.77	0.27	0.59	0.60	0.71	1.00				
Lu	0.05	0.59	0.21	0.92	0.80	0.62	0.78	0.24	0.57	0.58	0.68	1.00	1.00			
Hf	0.01	0.46	0.20	0.75	0.97	0.64	0.67	0.09	0.37	0.41	0.48	0.85	0.87	1.00		
Th	0.04	0.66	-0.36	0.40	0.22	0.76	0.46	0.39	0.44	0.32	0.44	0.39	0.39	0.36	1.00	
U	0.09	0.51	-0.24	0.42	0.22	0.65	0.41	0.42	0.46	0.35	0.47	0.40	0.39	0.33	0.83	1.00

Appendix A

Table R3 Results of Hf-Nd analyses of international rocks standards by MC-ICP-MS

	$^{143}Nd/^{144}Nd$	2SD	n	Ref.	$^{176}Hf/^{177}Hf$	2SD	n	Ref.
JB-3	0.513062	0.000013	2	0.513062[a]	0.283230	0.000011	2	0.283223[b]
JB-1	0.512779	0.000005	4	0.512782[b]	0.282963	0.000010	4	0.282965[b]
BHVO-2	0.512973	0.000010	4	0.512970[b]	0.283097	0.000011	4	0.283116[b]

Ref. = Reference values (http://www.minerals.cr.usgs.gov/geo_chem_stand). SD = standard deviation.

Appendix A

Table R2 Results of analyses of the international rocks standards (BHOV-2, GSR-1) and China National Standards Stream Sediments (GSD-9, GSD-10 and GSD-12) by ICP-MS.

	BHVO-2	Ref.[1]	GSR-1	Ref.[1]	GSD-10	Ref.[2]	GSD-12	Ref.[2]	GSD-9	Ref.[2]
Sc	31.6	32.0	6.05	6.10	3.65	4.10	5.28	5.10	10.5	11.1
V	318	317	22.4	24.0	106	107	44.4	47.0	96.4	97.0
Cr	281	280	3.05	5.00	142	136	34.1	35.0	89.2	85.0
Co	44.8	45.0	2.94	3.40	15.0	15.3	8.31	8.80	14.3	14.4
Ni	120	119	1.70	2.30	30.8	30.0	12.5	12.8	33.4	32.0
Rb	9.98	9.11	403	466	4.30	3.20	283	270	82.7	80.0
Sr	397	396	145	106	23.9	25.0	24.3	24.0	175	166
Y	26.2	26.0	69.6	62.0	11.7	14.0	25.0	29.0	22.2	27.0
Zr	170	172	182	167	57.0	70.0	196	234	318	370
Nb	18.4	18.1	40.7	40.0	5.72	6.80	14.9	15.4	15.3	18.0
Cs	0.101	0.100	38.4	38.4	2.04	2.30	7.71	7.90	4.67	5.10
Ba	132	131	349	343	37.1	42.0	199	206	430	430
La	15.3	15.2	54.3	54.0	12.0	13.0	28.3	32.7	38.9	40.0
Ce	37.2	37.5	109	108	37.5	58.0	58.7	61.0	79.5	78.0
Pr	5.18	5.35	13.0	12.7	2.78	3.20	6.54	6.00	8.88	9.20
Nd	24.5	24.5	48.2	47.0	11.2	11.8	24.0	26.0	33.9	34.0
Sm	6.06	6.07	9.40	9.70	2.26	2.40	4.76	5.00	6.24	6.30
Eu	2.03	2.07	0.857	0.850	0.474	0.470	0.708	0.610	1.49	1.33
Gd	6.10	6.24	9.27	9.30	2.79	2.20	5.49	4.40	7.04	5.50
Tb	0.926	0.920	1.80	1.65	0.400	0.420	0.802	0.820	0.927	0.870
Dy	5.26	5.31	11.1	10.2	2.14	2.20	4.63	4.80	4.73	5.10
Ho	0.968	0.980	2.34	2.05	0.428	0.450	0.979	0.940	0.930	0.960
Er	2.50	2.54	6.82	6.50	1.26	1.30	3.15	3.10	2.81	2.80
Tm	0.332	0.330	1.19	1.10	0.173	0.200	0.484	0.530	0.390	0.440
Yb	1.99	2.00	8.14	7.40	1.15	1.20	3.53	3.70	2.66	2.80
Lu	0.273	0.274	1.33	1.20	0.164	0.190	0.550	0.580	0.093	0.045
Hf	4.33	4.36	6.41	6.30	1.42	1.80	6.88	8.30	8.81	9.70
Ta	1.17	1.14	7.38	7.20	0.351	0.500	2.92	3.20	1.18	1.30
Pb	2.16	1.60	31.2	31.0	24.7	27.0	318	285	21.6	23.0
Th	1.24	1.22	55.7	54.0	5.29	5.00	21.5	21.4	12.5	12.4
U	0.419	0.403	19.6	18.8	2.22	2.10	8.59	7.80	3.11	2.60

Ref.[1] and Ref.[2] = Reference values.

1: http://www.minerals.cr.usgs.gov/geo_chem_stand;

2: Xia, X.J., Yan, M.C., Li, L.Z., Shen, H.J., 1985. Usable Values for Chinese Standard Reference Samples of Stream Sediments, Soils and Rocks: GSD9-12, GSS1-8 and GSR1-6. Geostandard Newsletter, V.IX, No.2, 277-280.

Appendix A

Table R1. Results of major element analyses of international rocks standards by XRF.

	GSR-1	SD (n=2)	Ref.	GSR-2	SD (n=3)	Ref.	GSR-3	SD (n=2)	Ref.	GSR-5	SD (n=4)	Ref.
SiO_2	72.92	0.03	72.83	60.57	0.18	60.62	44.79	0.25	44.64	59.16	0.07	59.23
TiO_2	0.29	0.01	0.29	0.52	0.01	0.52	2.33	0.06	2.36	0.67	0.01	0.66
Al_2O_3	13.59	0.02	13.40	16.22	0.20	16.17	13.68	0.19	13.83	18.82	0.13	18.82
CaO	1.55	0.12	1.55	5.23	0.03	5.20	8.89	0.02	8.81	0.67	0.11	0.60
Fe_2O_3	1.99	0.04	2.14	5.02	0.00	4.90	13.29	0.03	13.40	7.62	0.02	7.60
K_2O	4.85	0.11	5.01	1.84	0.02	1.89	2.37	0.01	2.32	4.23	0.06	4.16
MgO	0.49	0.07	0.42	1.76	0.01	1.72	7.45	0.29	7.77	2.08	0.06	2.01
MnO	0.05	0.01	0.06	0.07	0.00	0.08	0.16	0.01	0.17	0.02	0.02	0.02
Na_2O	3.08	0.02	3.13	3.88	0.03	3.86	3.44	0.19	3.38	0.35	0.01	0.35
P_2O_5	0.09	0.00	0.09	0.27	0.03	0.24	1.00	0.06	0.95	0.16	0.00	0.16

Ref. = Reference values (http://www.minerals.cr.usgs.gov/geo_chem_stand). SD = standard deviation. GSR-5 is one of the international shale standards.

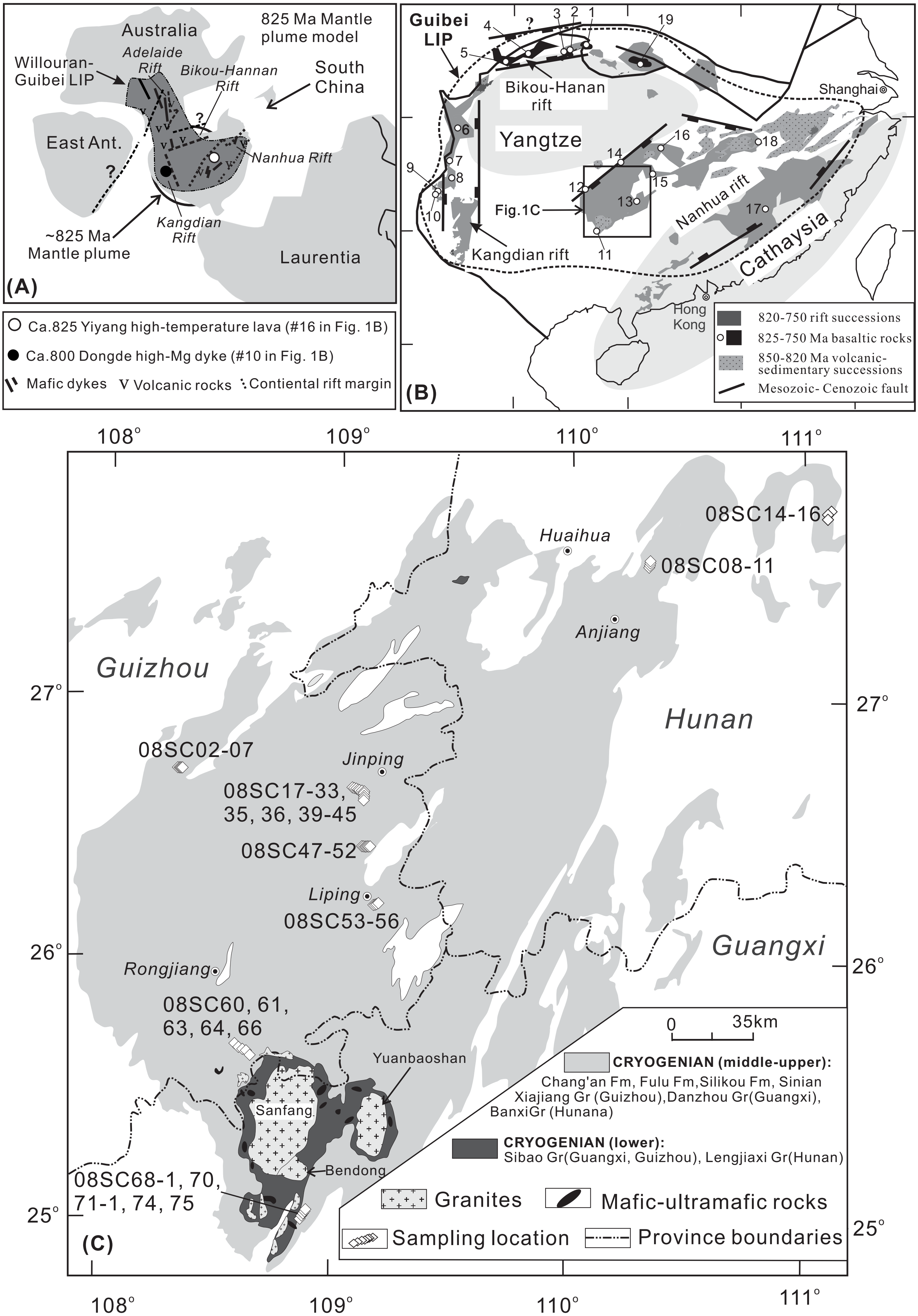
825 Ma Mantle plume model
Australia
Willouran-Guibei LIP
Adelaide Rift
Bikou-Hannan Rift
South China
East Ant.
Nanhua Rift
~825 Ma Mantle plume
Kangdian Rift
Laurentia
(A)
Ca.825 Yiyang high-temperature lava (#16 in Fig. 1B)
Ca.800 Dongde high-Mg dyke (#10 in Fig. 1B)
Mafic dykes
V Volcanic rocks
Contiental rift margin
Guibei LIP
Bikou-Hanan rift
Yangtze
Fig.1C
Kangdian rift
Nanhua rift
Cathaysia
Shanghai
Hong Kong
820-750 rift successions
825-750 Ma basaltic rocks
850-820 Ma volcanic-sedimentary successions
Mesozoic- Cenozoic fault
(B)
Guizhou
Hunan
Guangxi
Huaihua
Anjiang
Jinping
Liping
Rongjiang
Sanfang
Yuanbaoshan
Bendong
08SC14-16
08SC08-11
08SC02-07
08SC17-33, 35, 36, 39-45
08SC47-52
08SC53-56
08SC60, 61, 63, 64, 66
08SC68-1, 70, 71-1, 74, 75
0 35km
CRYOGENIAN (middle-upper):
Chang'an Fm, Fulu Fm,Silikou Fm, Sinian Xiajiang Gr (Guizhou),Danzhou Gr(Guangxi), BanxiGr (Hunana)
CRYOGENIAN (lower):
Sibao Gr(Guangxi, Guizhou), Lengjiaxi Gr(Hunan)
Granites
Mafic-ultramafic rocks
Sampling location
Province boundaries
(C)

Fig. 1

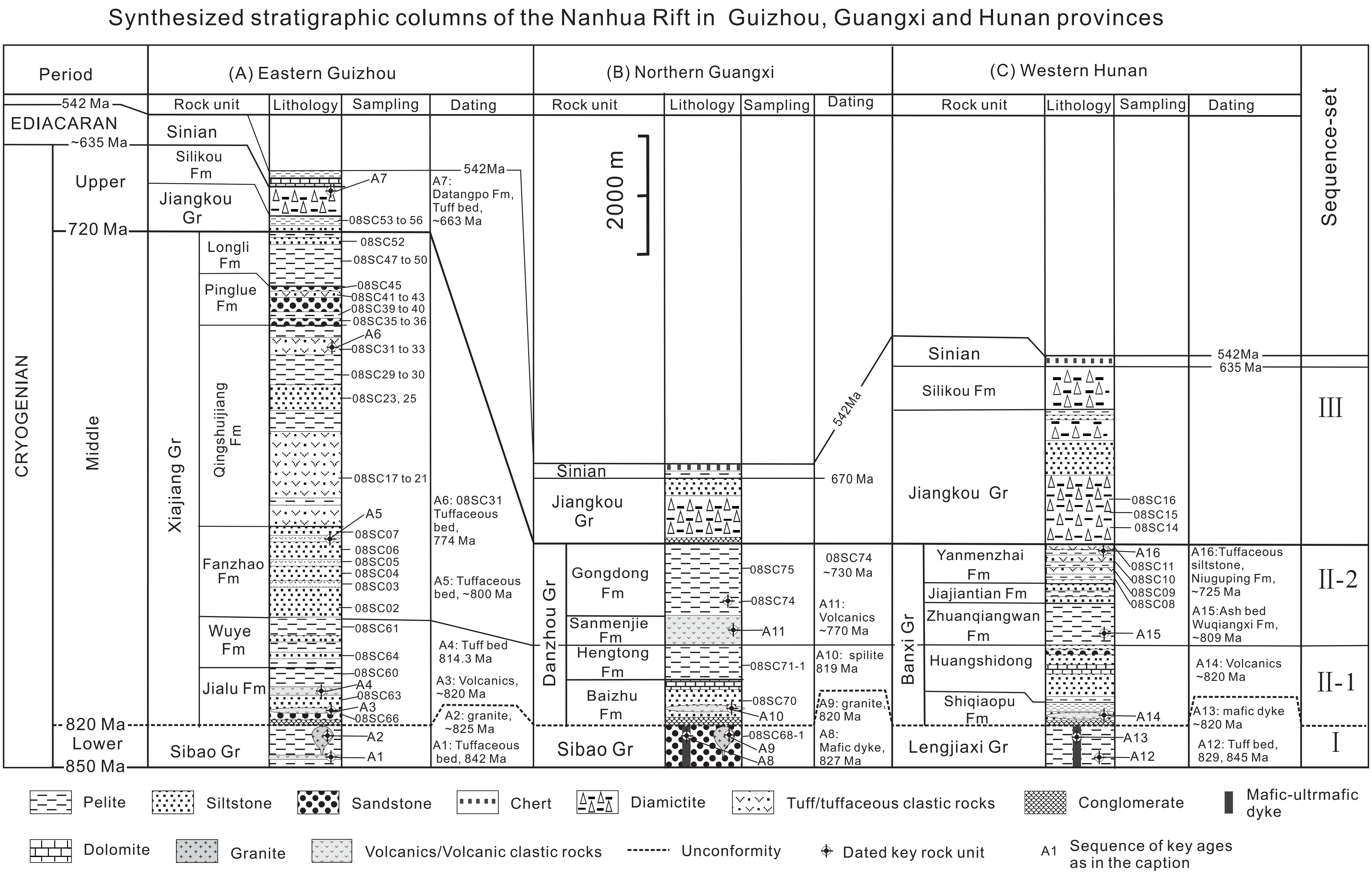
Synthesized stratigraphic columns of the Nanhua Rift in Guizhou, Guangxi and Hunan provinces
Period
(A) Eastern Guizhou
(B) Northern Guangxi
(C) Western Hunan
Sequence-set
Rock unit
Lithology
Sampling
Dating
542 Ma
EDIACARAN
~635 Ma
CRYOGENIAN
Upper
Middle
Lower
720 Ma
820 Ma
850 Ma
Sinian
Silikou Fm
Jiangkou Gr
Xiajiang Gr
Longli Fm
Pinglue Fm
Qingshuijiang Fm
Fanzhao Fm
Wuye Fm
Jialu Fm
Sibao Gr
A7
08SC53 to 56
08SC52
08SC47 to 50
08SC45
08SC41 to 43
08SC39 to 40
08SC35 to 36
A6
08SC31 to 33
08SC29 to 30
08SC23, 25
08SC17 to 21
A5
08SC07
08SC06
08SC05
08SC04
08SC03
08SC02
08SC61
08SC64
08SC60
A4
08SC63
A3
08SC66
A2
A1
542Ma
A7: Datangpo Fm, Tuff bed, ~663 Ma
A6: 08SC31 Tuffaceous bed, 774 Ma
A5: Tuffaceous bed, ~800 Ma
A4: Tuff bed 814.3 Ma
A3: Volcanics, ~820 Ma
A2: granite, ~825 Ma
A1: Tuffaceous bed, 842 Ma
2000 m
Sinian
Jiangkou Gr
Danzhou Gr
Gongdong Fm
Sanmenjie Fm
Hengtong Fm
Baizhu Fm
Sibao Gr
08SC75
08SC74
A11
08SC71-1
08SC70
A10
08SC68-1
A9
A8
542Ma
670 Ma
08SC74 ~730 Ma
A11: Volcanics ~770 Ma
A10: spilite 819 Ma
A9: granite, 820 Ma
A8: Mafic dyke, 827 Ma
Sinian
Silikou Fm
Jiangkou Gr
Banxi Gr
Yanmenzhai Fm
Jiajiantian Fm
Zhuanqiangwan Fm
Huangshidong
Shiqiaopu Fm
Lengjiaxi Gr
08SC16
08SC15
08SC14
A16
08SC11
08SC10
08SC09
08SC08
A15
A14
A13
A12
542Ma
635 Ma
A16:Tuffaceous siltstone, Niuguping Fm, ~725 Ma
A15:Ash bed Wuqiangxi Fm, ~809 Ma
A14: Volcanics ~820 Ma
A13: mafic dyke ~820 Ma
A12: Tuff bed, 829, 845 Ma
III
II-2
II-1
I
Pelite
Siltstone
Sandstone
Chert
Diamictite
Tuff/tuffaceous clastic rocks
Conglomerate
Mafic-ultrmafic dyke
Dolomite
Granite
Volcanics/Volcanic clastic rocks
Unconformity
Dated key rock unit
A1 Sequence of key ages as in the caption

Fig. 2

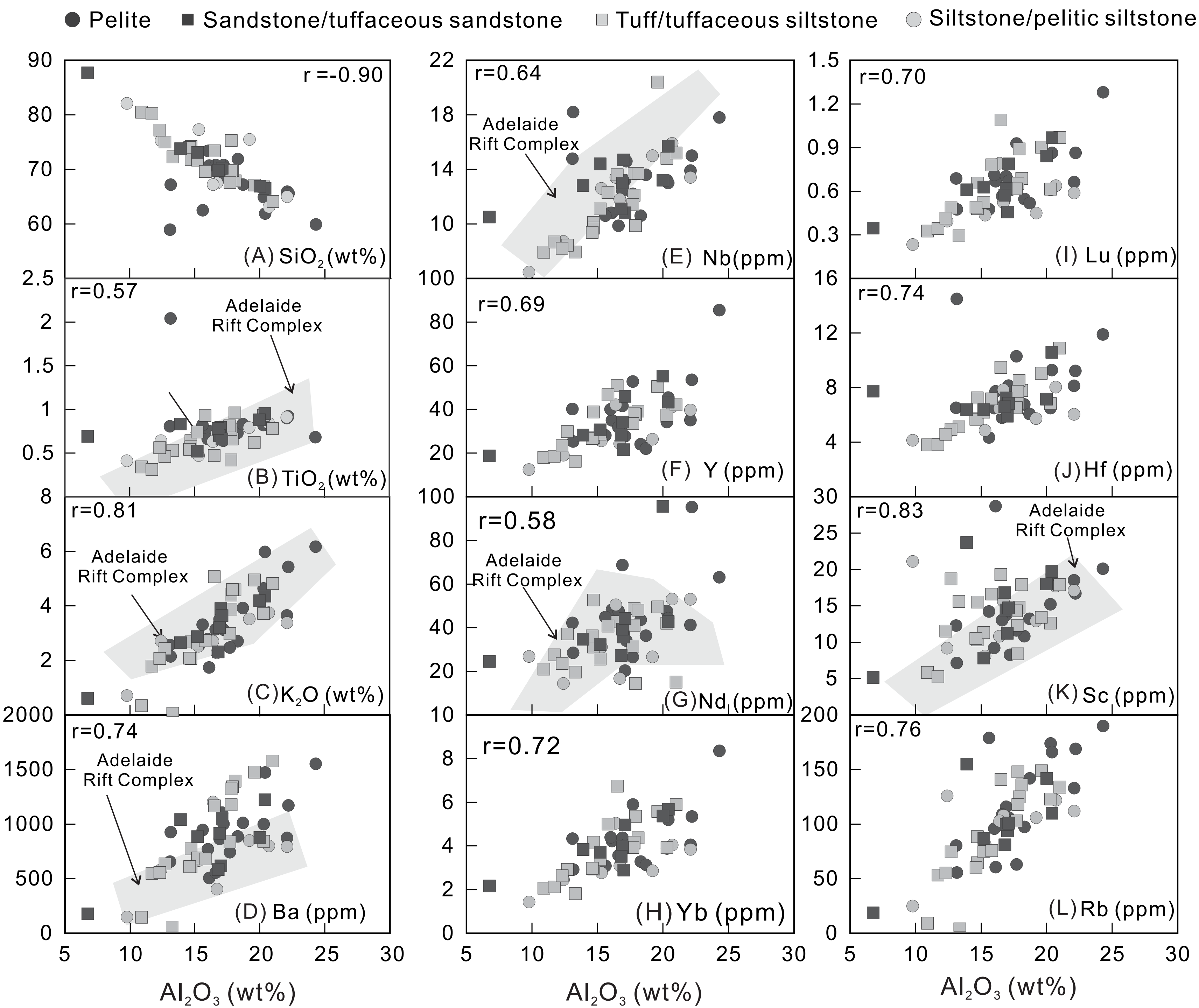
Pelite
Sandstone/tuffaceous sandstone
Tuff/tuffaceous siltstone
Siltstone/pelitic siltstone
r =-0.90
(A) SiO2 (wt%)
r=0.57
Adelaide Rift Complex
(B) TiO2 (wt%)
r=0.81
Adelaide Rift Complex
(C) K2O (wt%)
r=0.74
Adelaide Rift Complex
(D) Ba (ppm)
r=0.64
Adelaide Rift Complex
(E) Nb (ppm)
r=0.69
(F) Y (ppm)
r=0.58
Adelaide Rift Complex
(G) Nd (ppm)
r=0.72
(H) Yb (ppm)
r=0.70
(I) Lu (ppm)
r=0.74
(J) Hf (ppm)
r=0.83
Adelaide Rift Complex
(K) Sc (ppm)
r=0.76
(L) Rb (ppm)
Al2O3 (wt%)
Al2O3 (wt%)
Al2O3 (wt%)

Fig. 3

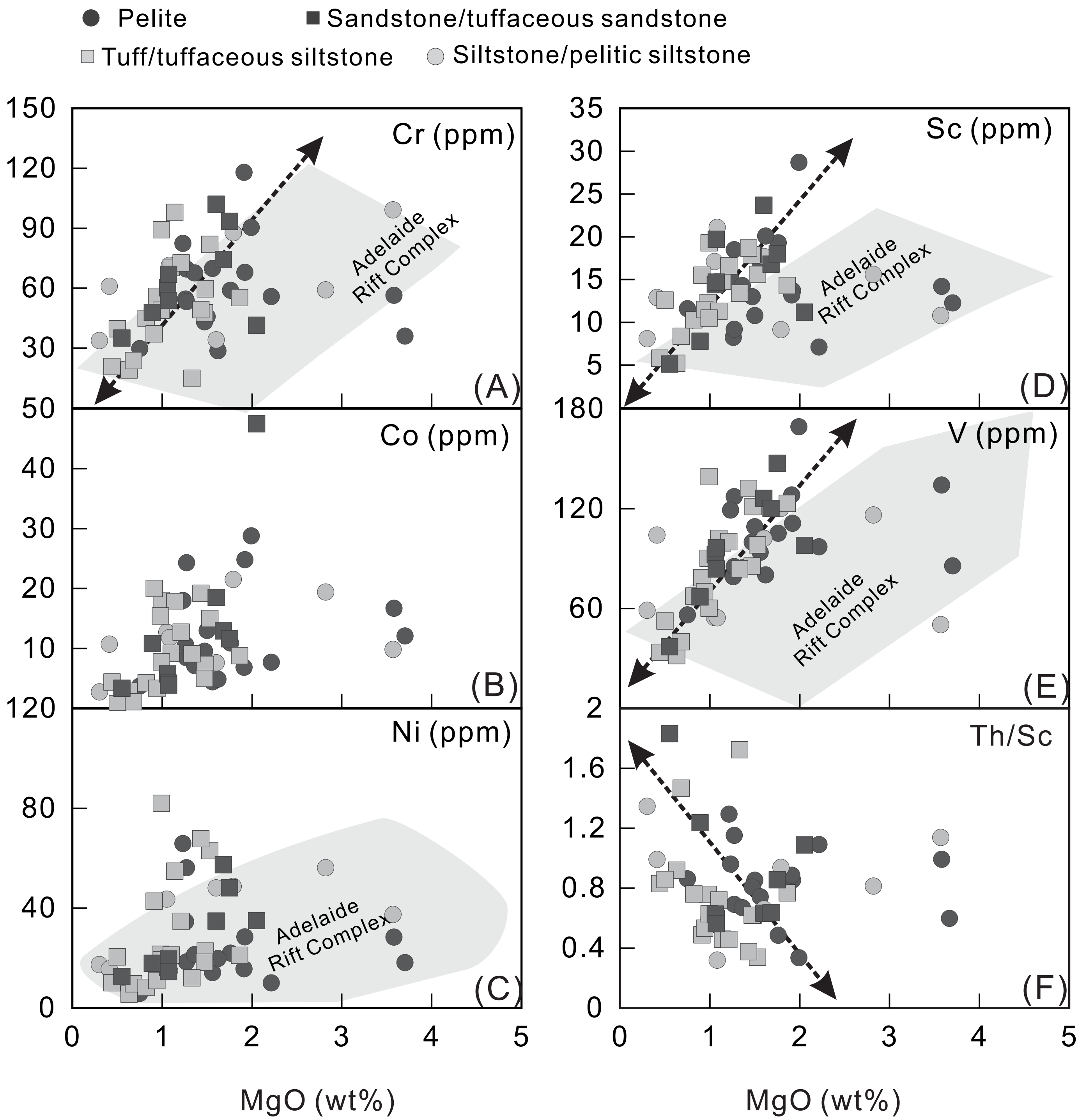

Pelite
Sandstone/tuffaceous sandstone
Tuff/tuffaceous siltstone
Siltstone/pelitic siltstone
Cr (ppm)
Adelaide Rift Complex
(A)
Sc (ppm)
Adelaide Rift Complex
(D)
Co (ppm)
(B)
V (ppm)
Adelaide Rift Complex
(E)
Ni (ppm)
Adelaide Rift Complex
(C)
Th/Sc
(F)
MgO (wt%)
MgO (wt%)

Fig. 4

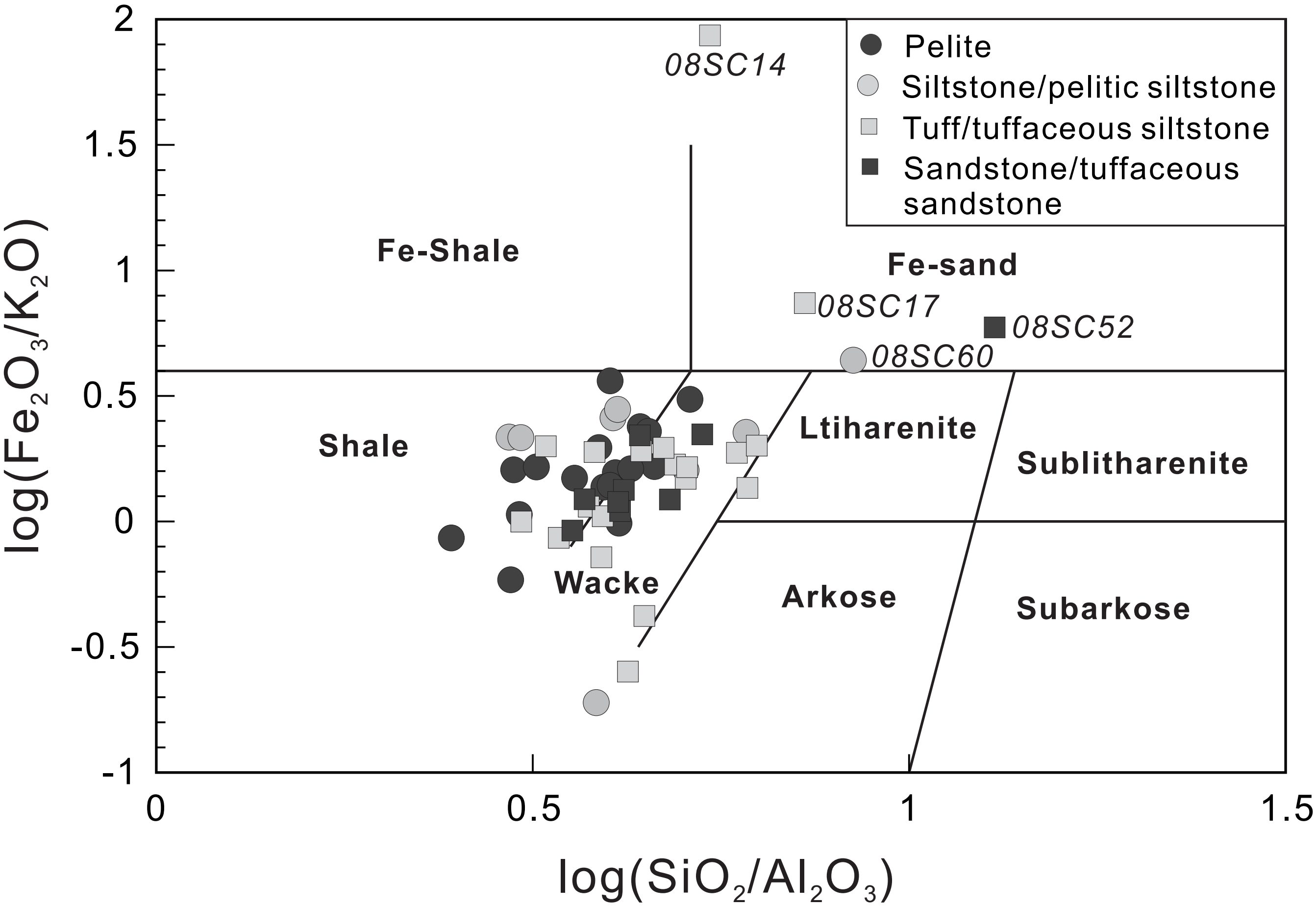
08SC14
Pelite
Siltstone/pelitic siltstone
Tuff/tuffaceous siltstone
Sandstone/tuffaceous sandstone
Fe-Shale
Fe-sand
08SC17
08SC52
08SC60
Shale
Ltiharenite
Sublitharenite
Wacke
Arkose
Subarkose
2
1.5
1
0.5
0
-0.5
-1
0
0.5
1
1.5
log(Fe2O3/K2O)
log(SiO2/Al2O3)

Fig. 5

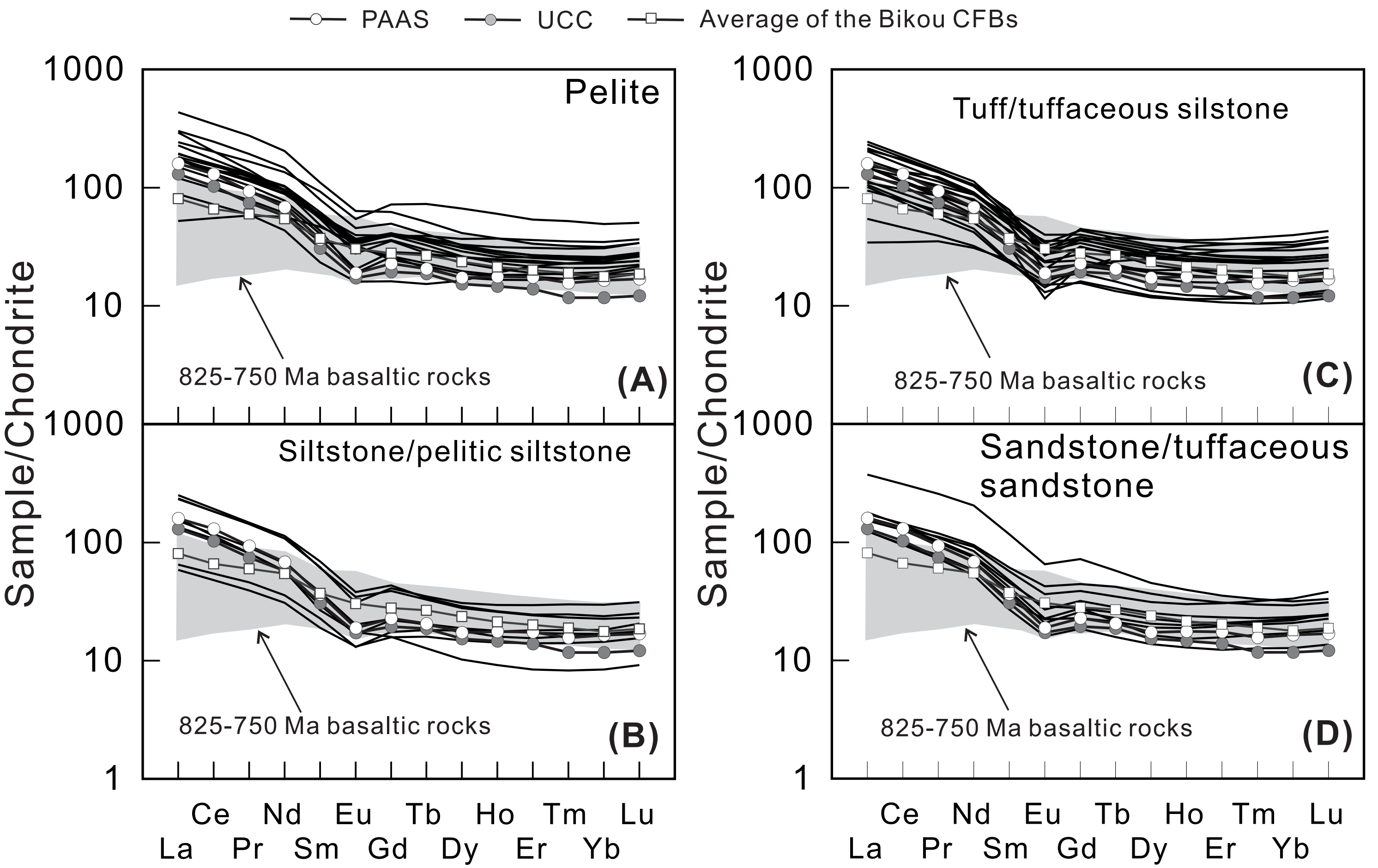

PAAS
UCC
Average of the Bikou CFBs
Pelite
(A)
Tuff/tuffaceous silstone
(C)
Siltstone/pelitic siltstone
(B)
Sandstone/tuffaceous sandstone
(D)
825-750 Ma basaltic rocks
Sample/Chondrite
1000
100
10
1
La Ce Pr Nd Sm Eu Gd Tb Dy Ho Er Tm Yb Lu

Fig. 6

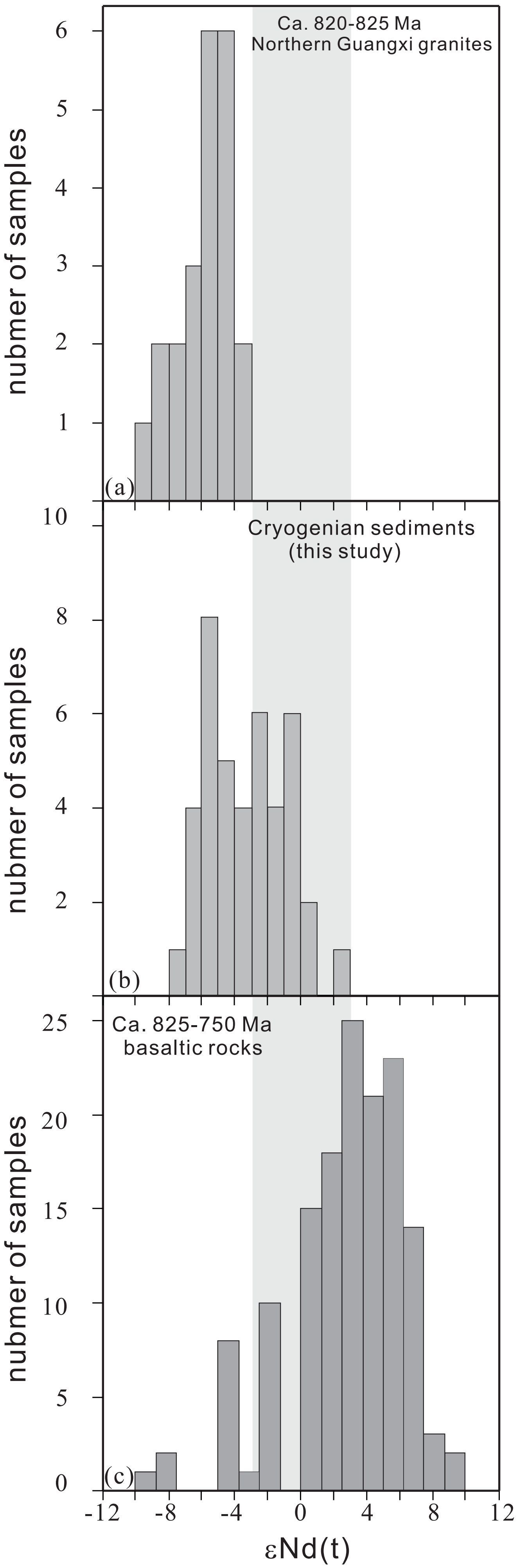

Ca. 820-825 Ma
Northern Guangxi granites
(a)
Cryogenian sediments
(this study)
(b)
Ca. 825-750 Ma
basaltic rocks
(c)
nubmer of samples
εNd(t)
-12
-8
-4
0
4
8
12

Fig. 7

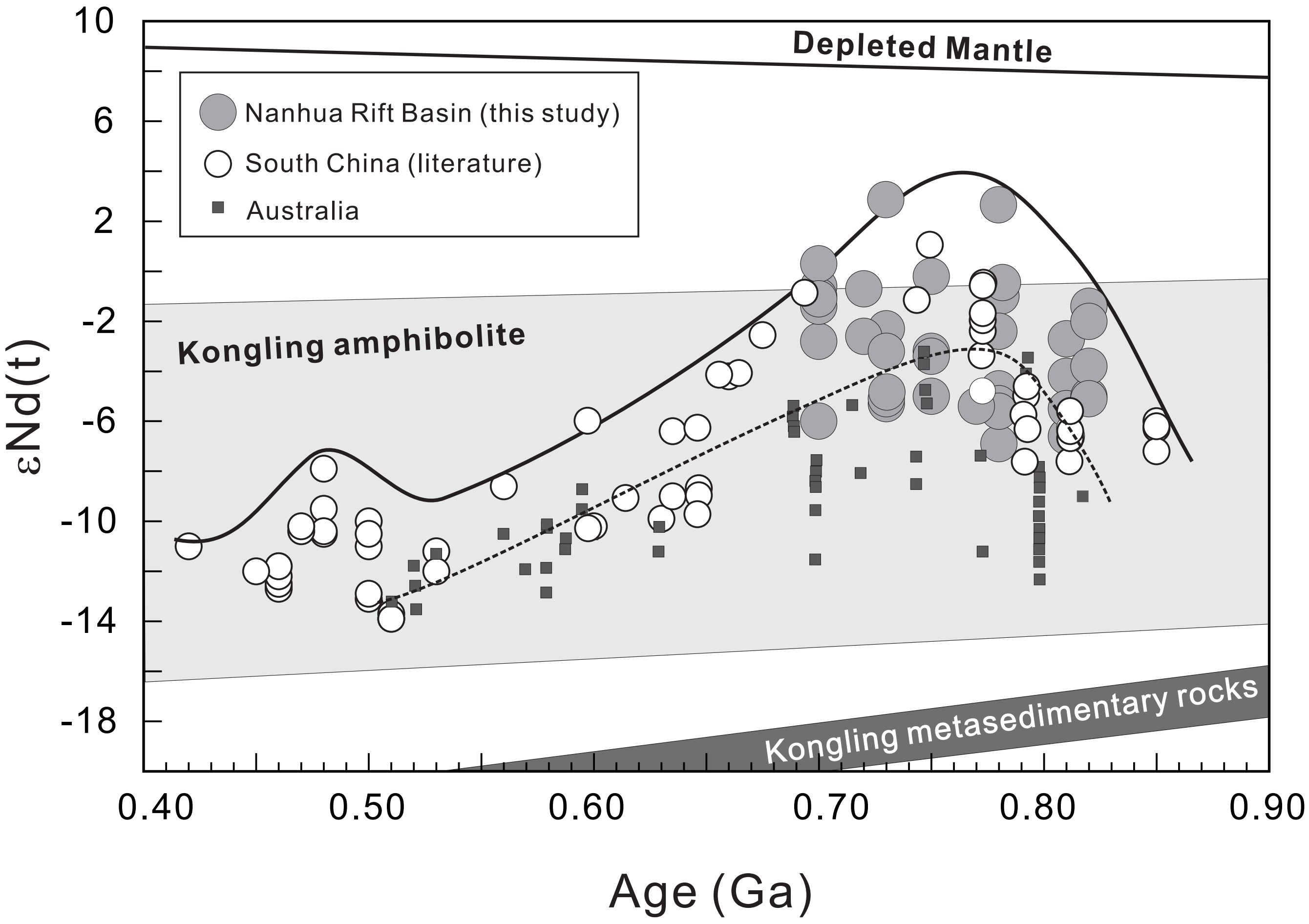

Depleted Mantle
Nanhua Rift Basin (this study)
South China (literature)
Australia
Kongling amphibolite
Kongling metasedimentary rocks
10
6
2
-2
-6
-10
-14
-18
εNd(t)
0.40
0.50
0.60
0.70
0.80
0.90
Age (Ga)

Fig. 8

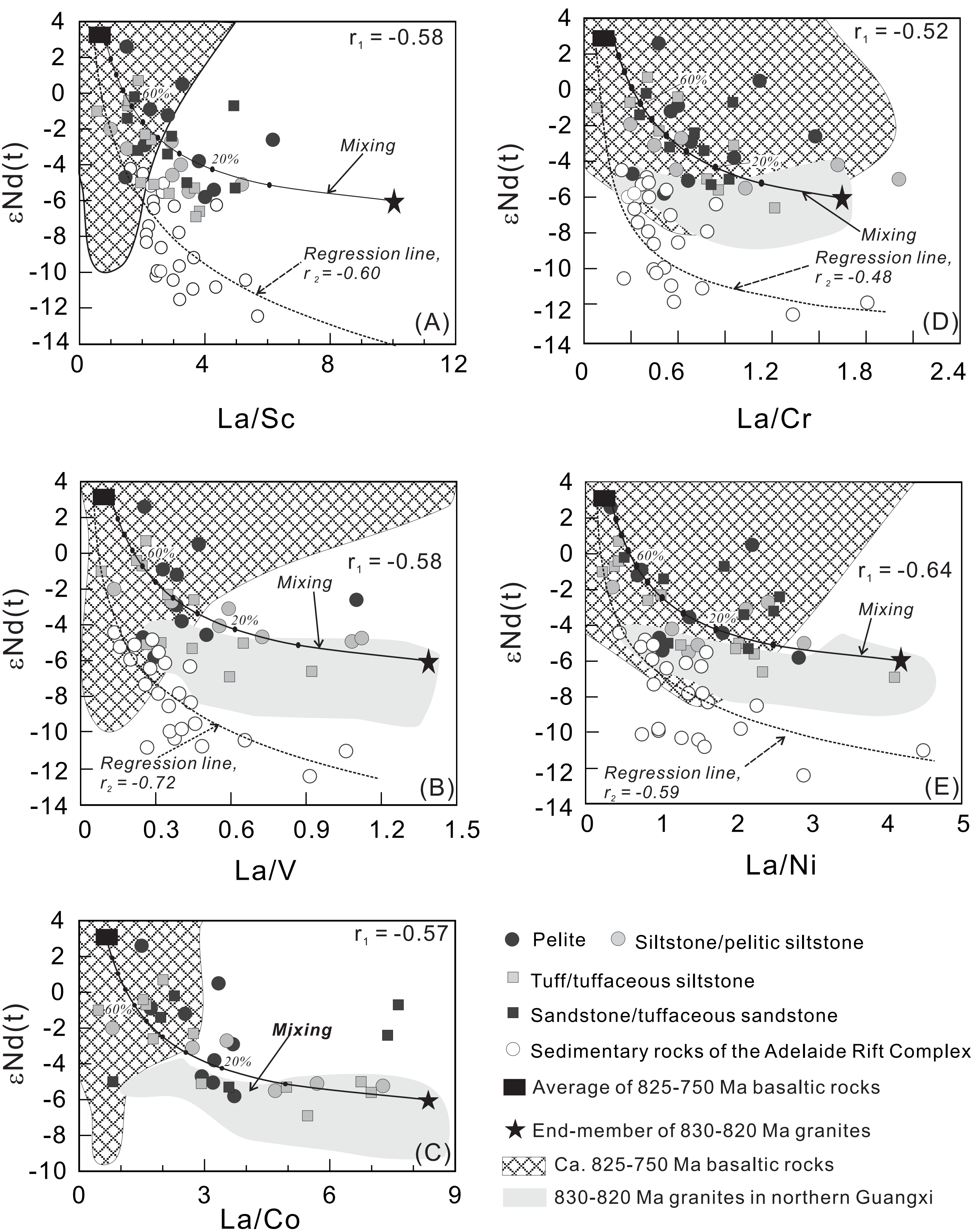

εNd(t)
La/Sc
r1 = -0.58
Mixing
Regression line,
r2 = -0.60
60%
20%
(A)
La/Cr
r1 = -0.52
r2 = -0.48
(D)
La/V
r1 = -0.58
r2 = -0.72
(B)
La/Ni
r1 = -0.64
r2 = -0.59
(E)
La/Co
r1 = -0.57
(C)
Pelite
Siltstone/pelitic siltstone
Tuff/tuffaceous siltstone
Sandstone/tuffaceous sandstone
Sedimentary rocks of the Adelaide Rift Complex
Average of 825-750 Ma basaltic rocks
End-member of 830-820 Ma granites
Ca. 825-750 Ma basaltic rocks
830-820 Ma granites in northern Guangxi

Fig. 9

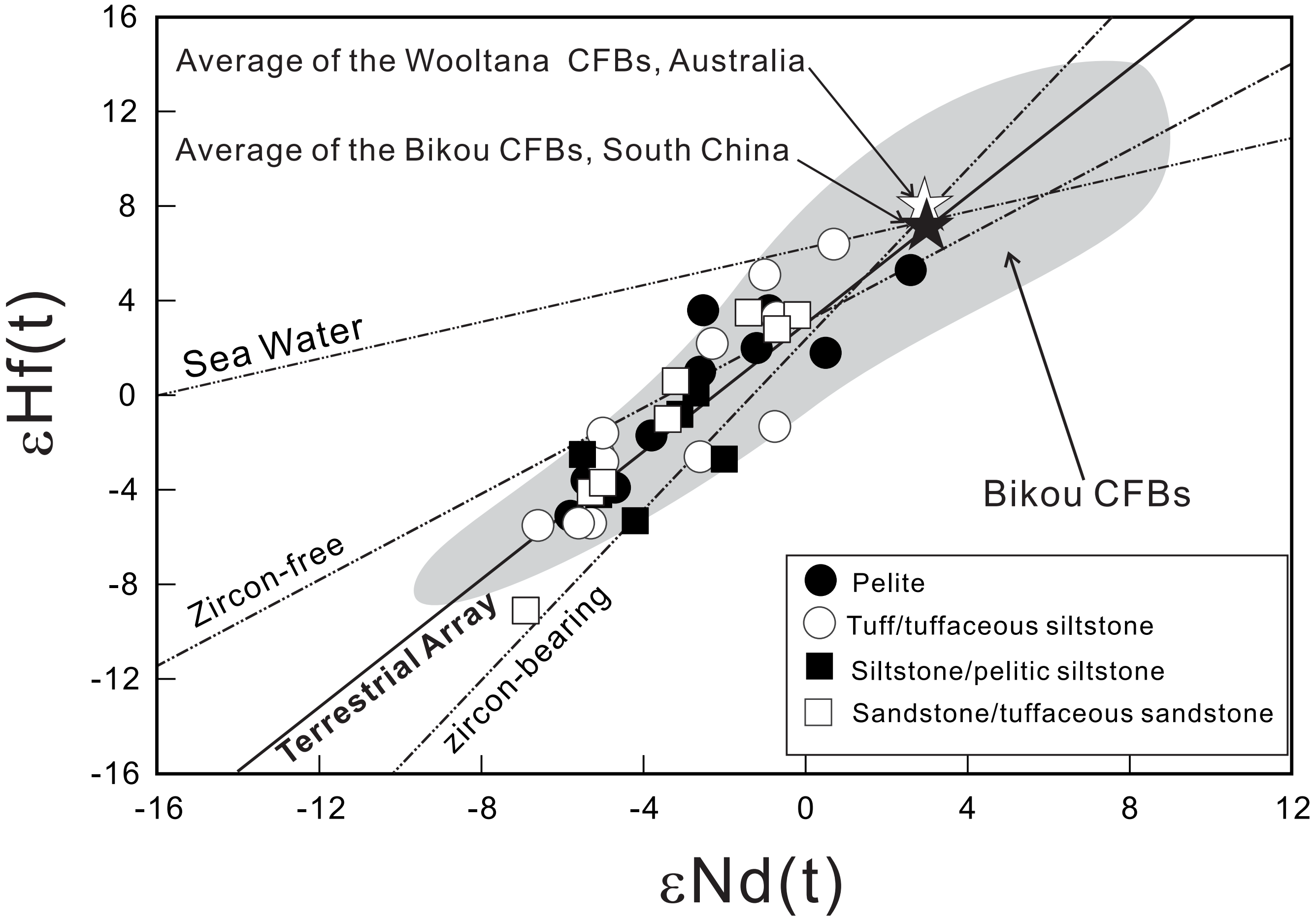

Average of the Wooltana CFBs, Australia
Average of the Bikou CFBs, South China
Sea Water
Zircon-free
Terrestrial Array
zircon-bearing
Bikou CFBs
Pelite
Tuff/tuffaceous siltstone
Siltstone/pelitic siltstone
Sandstone/tuffaceous sandstone
εHf(t)
εNd(t)
16
12
8
4
0
-4
-8
-12
-16
-16
-12
-8
-4
0
4
8
12

Fig. 10

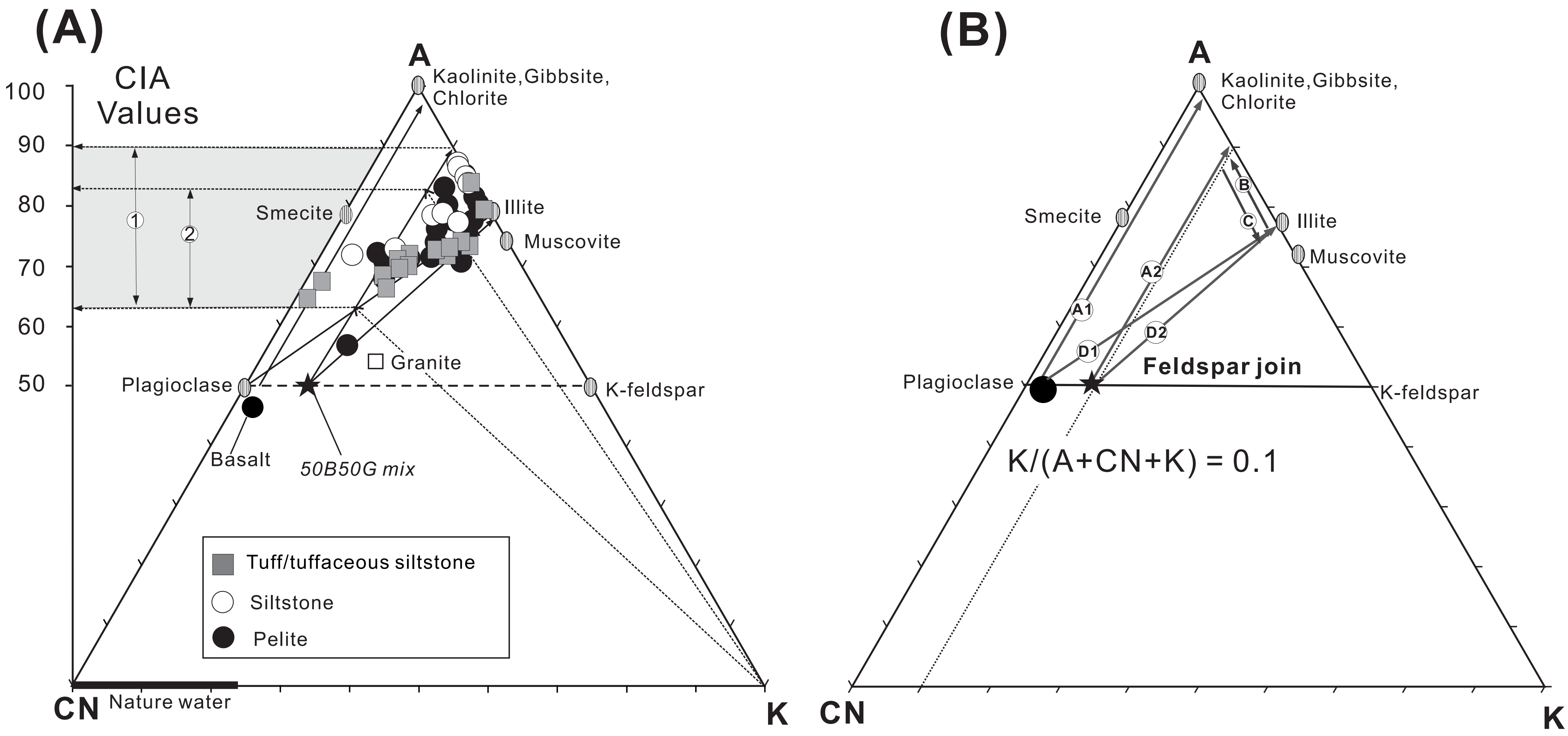
(A)
CIA
Values
100
90
80
70
60
50
A
Kaolinite,Gibbsite,
Chlorite
Smecite
Illite
Muscovite
Plagioclase
K-feldspar
Granite
Basalt
50B50G mix
Tuff/tuffaceous siltstone
Siltstone
Pelite
CN
Nature water
K
(B)
A
Kaolinite,Gibbsite,
Chlorite
Smecite
Illite
Muscovite
A1
A2
B
C
D1
D2
Plagioclase
Feldspar join
K-feldspar
K/(A+CN+K) = 0.1
CN
K

Fig. 11